Title
Validation of a computer-aided approach to three-dimensional craniofacial imaging

Author
Quintero, Juan-Carlos,

Publication Date
1998

Peer reviewed|Thesis/dissertation

VALIDATION OF A COMPUTER-AIDED APPROACH TO THREE -DIMENSIONAL CRANIOFACIAL IMAGING

by

Juan-Carlos Quintero

THESIS

Submitted in partial satisfaction of the requirements for the degree of

MASTER OF SCIENCE

in

ORAL BIOLOGY

in the

GRADUATE DIVISION

of the

UNIVERSITY OF CALIFORNIA

San Francisco

Date University Librarian

Degree Conferred: . . . . . .

ACKNOWLEDGMENT

I would like to express my sincere gratitude to Dr. David Hatcher for being the driving force and guidance of this project. His enthusiasm and vision for developing improved craniofacial imaging methods have been both inspirational and contagious. I would like to thank Dr. Hassan Mostafavi for his technical expertise and support throughout the project. I thank Mr. Gary Cason for his early contribution in the pilot stage of the project and Mr. Craig Dial from Diagnostic Digital Imaging (DDI) for his vital assistance in the image acquisition processes. I thank Acuscape Corporation for creating, developing and providing the hardware and software to make this project possible.

I would like to express my gratitude to my committee members, including Dr. Charles McNeill, Dr. Arthur Miller, and Dr. Karin Vargervik for their guidance in the development of this project and for their input in the final form of this manuscript. It has been a privilege to work with such leaders in their fields.

I would like to thank Dr. Stuart Gansky for his invaluable statistical expertise and his contributions to the design and analysis of this project in all its stages. This thesis was made possible with his time, patience and effort.

I would like to thank Dr. Sean Carlson for his assistance during various times of the project. It is truly a privilege to have such a co-resident serve as a teacher, colleague and friend. I also wish to thank Dr. Shelly Baumrind for inspiring me with his work in stereophotogrammetry and for laying the basic framework for my understanding of this science.

Finally, I would like to express my sincere appreciation to my family for all their love and support throughout my entire life, and to Tessie for her enduring love and support.

TABLE OF CONTENTS

LIST OF TABLES

LIST OF FIGURES

I. INTRODUCTION

A. BACKGROUND & SIGNIFICANCE

Historically, imaging modalities in orthodontics have been based on the technology available preceding their development, regardless of the inherent flaws and limitations of the techniques on which they are based. But what exactly is the purpose of craniofacial imaging? What if imaging modalities could be developed to fulfill the desired ideal principles and goals they were intended to fulfill? Although highly hypothetical, what if we were not limited by previous technology in the selection of our diagnostic imaging modalities? In order to answer these questions, it is useful to understand the reality of traditional cephalometry, along with its benefits, and more importantly its limitations.

Cephalometry (the measurement of the head), was developed as an anthropological technique to quantify shape & sizes of skulls. The discovery of x-rays by Roentgen in 1895 revolutionized medicine and dentistry. Traditional cephalometry in two dimensions, known as roentgenographic cephalometry, was introduced in 1931 by Broadbent to the dental profession, and has since remained relatively unchanged[1]. A limitless potential for cephalograms both as a clinical and research tool for the study of craniofacial growth, development, and treatment results has been suggested[2]. However, orthodontics has based much of its clinical evidence and treatment modalities on erroneous assumptions inherent to the technique used in traditional two-dimensional cephalometry.

There exists a wide spectrum of limitations in two-dimensional cephalometry leading to questions concerning the validity of its scientific value and thus, its application[3-5]. Firstly, and perhaps of most significance, is

that a conventional headfilm is a two dimensional representation of a three-dimensional object. There exist differential projective displacements of anatomic structures lying three-dimensionally at different planes within the head, which are projected two-dimensionally[6]. Secondly, the two-dimensional nature of the cephalogram requires that anatomic landmarks of the left and right halves be mirror images of each other at the midsagittal plane[7]. This assumption is rarely satisfied and is not at all useful for assessment of craniofacial anomalies and facial asymmetries. Thirdly, a significant amount of external error is associated with image acquisition, known as radiographic projection errors. These include size magnification and distortion, errors in patient positioning, and projective distortion inherent to the film/patient/focus geometric relationships. Fourthly, errors within the human measuring system relating to manual data collection and processing have been shown to be quite high as these have a low reliability[8]. Additionally, there are errors associated with inherent ambiguity in locating anatomical landmarks due to the lack of well-defined outlines, hard edges, and shadows and variation in patient position[6]. Landmark identification errors have been considered to be the major source of cephalometric error[9-11].

Many cephalometric analyses have been developed to help diagnose skeletal malocclusions and dentofacial deformities. However, several investigators have seriously questioned their scientific value[12-14]. Vig has reported on the lack of validity that cephalometric analyses have as a diagnostic instrument, and demonstrated that conclusions drawn on the basis of the same cephalograms may vary significantly depending on the analysis used[15]. This has been emphasized by Baumrind who has concluded after several investigations that the manner in which the data are interpreted is more critical than the reproducibility of landmark location or even the

biologically-based changes of the areas with respect to which structural superimpositions are defined[16-20]. The cumulative errors associated with traditional two-dimensional cephalometry have been reported to be significant enough to affect diagnosis and treatment decisions in some cases[5, 21].

Hatcher has recently reviewed and categorized sources of error inherent to most imaging techniques used in traditional cephalometrics, including internal and external orientation and geometric and association errors, as follows[22] :

Internal orientation error. This refers to the three-dimensional attitude of the patient relative to the central x-ray beam or imaging device.

External orientation. This refers to the three-dimensional spatial relationship or alignment of the imaging device, patient stabilizing device, and the image-recording-device.

Geometric error. This primarily refers to the differential magnification of the projection distance created among the imaging device, recording device, and a three-dimensional object. For example, structures farthest from the film will be magnified more than objects closer to the film. In addition, divergence of the x-ray beam from its source to the recording device will result in misrepresentation of anatomy.

Association error. This refers to the difficulty in identifying a three-dimensional point in two or more projections acquired from different points of view. The difficulty in identifying the identical point on two or more images is proportional to an increase in the divergence angle between the projections.

Therefore, in the hopes of eliminating these random and systematic errors, methods have been developed to provide three-dimensional

representation of the craniofacial complex. The first effort was proposed by Broadbent and Bolton, who originally introduced the roentgenographic cephalogram and stressed the importance to represent the three-dimensional nature of the head [1, 23]. They described the Orientator, which attempted to coordinate landmarks determined from the lateral and posterior anterior headfilms back to three dimensional space. However, the Orientator was not free of the flaws and limitations inherent to two-dimensional cephalograms. Baumrind has reported on the error of the Orientator method, due to variations in identification of identical landmarks from two different cephalograms and differential enlargements of the two views[24]. More contemporary efforts include computer aided tomography (CAT scans), computer aided design (CAD) software and a mathematical or biorthogonal geometric approach known as tensor analysis[25-27]. However, their economical and biological cost, and the poor to none image rendering, respectively, do not make them practical for ordinary clinical use in orthodontics.

The principle of coplanar stereometry has been used for almost a century in the production of terrestrial maps from aerial photographs. The principle of this technique was introduced to modern craniofacial imaging by Baumrind, and Moffit who developed a stereophotogrammetric approach to three-dimensional cephalometry from coplanar stereo pairs images[24, 28]. The limitation of this approach has been the expensive construction of the stereophotogrammetric machinery and the external orientation error introduced by patient movement during the acquisition of the two coplanar stereo films.

B. GOALS & PRINCIPLES OF CRANIOFACIAL IMAGING

Returning to the original problem, it is recognizable that a substantial portion of the orthodontic database has been constructed on the inherent inappropriateness and error proneness of traditional cephalometrics, as it has been the most frequently applied quantitative method within orthodontic research[6]. According to the biometrician Fred Bookstein, traditional cephalometrics has neither valid biologic parameters nor valid biometric predictions. In an essay he recently wrote[14]:

> "The {orthodontic} profession's collective research effort of recent decades has resulted in no discoveries of biological parameters having any validity in the clinical context of conventional orthodontic care."

In general, the purpose of imaging is to help solve specific clinical problems. As applied to the complex relations of craniofacial diagnosis, growth and treatment, either for the purpose of scientific investigation or for strict clinical application, the goals of orthodontic craniofacial imaging should fall into the following categories:

1) Assessment of pathology and deviation from norms
2) Estimation of expected growth
3) Evaluation of preceding growth
4) Comparison of different treatment methods, on different facial types, and at different maturational stages.
5) Subtraction of treatment effects from expected unaltered growth and/or development

The ideal imaging modality is the one which maximizes the desired information and minimizes the physiological risk and economical cost to the patient. The underlying principle of *ideal* imaging which must be met is the

determination of anatomic truth in terms of accurate portrayal of spatial orientation, size, shape, form, and relationships of desired structures or features[22]. This requires assessment in three planes of space as craniofacial form is defined three-dimensionally. Bookstein has emphasized the loss of information about shape which takes place when a three-dimensional structure is represented by a set of two-dimensional coordinates because of the discarded directional data on the associations among landmarks that lie along any given anatomical edge or surface[29].

C. PRINCIPLES OF MODERN PHOTOGRAMMETRY [30]

The field of civil engineering has developed standard aerial mapping techniques to measure three-dimensional relationships of objects and terrains. One of these techniques, known as stereophotogrammetry, attempts to solve the problem of three dimensional measurements from two-dimensional views or projections [31]. An example of its application is in the construction of terrestrial maps from multiple aerial photographs, where imaging parameters such as angles, focal lengths, film-to-object distances, and marker to marker distances are surveyed and known. This allows for mathematical and highly accurate reconstructions or "mapping" of terrains. Its simulation and application to craniofacial imaging using radiographic films has been developed by several investigators[24, 31-34].

Although the science of photogrammetry as applied to map-making has been around for some time, the use of nontopographic photogrammetry for industrial and architectural measurements has grown only in the last decade[35]. Recent developments like digital cameras and improved video technology has greatly benefited this growing area. The previous work in three-dimensional skull mapping has not utilized the full potential of non-

topographic photogrammetry. The methods have been limited to simple triangulation after associating easily identifiable landmarks in two or more X-rays. Furthermore, the geometric calibration techniques have not used the new techniques that are more accurate and convenient, and at the same time can utilize the on-line potential of computer workstations. For example, using the "bundle adjustment method" developed by the photogrammetrist D. C. Brown, both the geometric calibration and three-dimensional mapping functions can be made more elegant and accurate[36]. This is a self-calibrating method that uses a large number of measurement points simultaneously in the non-linear estimation problem that estimates the camera position and orientation as well as the desired point coordinates.

D. ADVANCED IMAGING [30]

One of the most significant limitations of conventional imaging modalities in maxillofacial radiology has been the lack of practical, cost-effective methods to represent anatomic truth. Craniofacial imaging is three-dimensional in nature, and there has been difficulty in identifying a three-dimensional point in two or more projections acquired from different points of view [24, 28].

Digital imaging offers the opportunity for mathematical manipulation of image data through the use of algorithms which perform various functions. Advances in computer hardware such as more powerful processors, image input devices, and high resolution large screen monitors allow for practical and convenient "soft copy" image exploitation [22].

A limitation of previous stereophotogrammetric approaches to three-dimensional cephalometrics has been the previously discussed "association error". This difficulty of identifying an identical three-dimensional point on

two or more images is proportional to the divergence of the angle between the two projections. Until recently, only CT scans offered a solution to this problem by sampling a large number of small angle increments around the object, after which any given "feature" is correctly located as a result of the mathematical image reconstruction process itself [22]. The financial cost and radiation exposure limits its use as a routine diagnostic tool.

Modern photogrammetry can be applied to solve accurate three-dimensional skull mapping by using a "bundle adjustment method", in which both the geometric calibration and three dimensional mapping functions can be accurate [36]. This self-calibration method uses a large number of measurement points simultaneously to calculate the position of the imaging device and subsequently, three-dimensional spatial coordinates of the anatomic features.

Identifying landmarks, three-dimensionally, allows for tracking changes of landmarks due to growth, development, movement, and orthodontic or surgical treatment. This same tracking technology can be applied to other clinical data collection methods such as photographic, tomographic, MRI, and CT multiplanar images. Since image acquisition includes a common calibration frame, images can be spatially correlated and integrated together and even utilized to include motion with timed sequence of video images. Image registration occurs by fusing data to a common three-dimensional coordinate system through the use of common surveyed reference markers. The spatial and temporal referencing to a common coordinate system of these independently acquired images, allows for data fusion to create a resulting single three-dimensional composite image.

E. INNOVATIVE APPROACH TO THREE-DIMENSIONAL CRANIOFACIAL IMAGING[30]

The advent of digital technology has recently given an impulse of validity to cephalometry by eliminating much of the error associated with image acquisition and landmark identification apparent in traditional cephalometry, thus, allowing for highly accurate three-dimensional image acquisition.

By combining digital technology with modern stereophotogrammetry, a digital replica of a patient is now possible by computer-aided fusion of radiographic and/or photographic images. The image acquisition process of this system includes a built-in, inherent calibration technique which automatically corrects for external errors. This technology allows accurate three-dimensional modeling of hard and soft tissue anatomical landmarks from multiple cephalometric films and photographs. Sculptor™ (Acuscape, Corporation, Quail Ridge Center, 1200 E. Alosta Ave, Glendora, Ca 91740), which is the software developed as a result of this technology, combines modern digital photogrammetry with image analysis in a workstation environment based on Windows PC. The main advantages and features of Sculptor™ are indicated below in the next paragraph.

The software computes accurate skull three-dimensional landmark locations and cephalometric traces, including three-dimensional curving forms such as jaws, orbital rims, mandibular canal, crqanial base, sella turcica, temporomandibular joints and alveolar ridges. It merges two or more cephalometric type headfilms acquired at approximately prescribed head orientations into a single accurate three-dimensional database of anatomic structures. The computed traces and landmarks are displayed in virtual view with the ability to interactively change the viewing angle.

A unique self-calibration feature of the software, based on advanced digital imaging and photogrammetry algorithms, eliminates the need for a head fixation mechanism of the cephalostat while compensating for all magnification and rotation effects. This calibration technique further allows geometric cross-calibration of the visible band images such as digital color photographs and video frames with the scanned cephalometric films. This provides the capability to superimpose 3-D hard tissue landmarks and traces onto digital photographs or captured video frames of the face with accurate registration to the photographic view.

F. PURPOSE, SPECIFIC AIMS, AND NULL HYPOTHESIS

1. PURPOSE

The purpose of this study was to evaluate the accuracy and precision of an innovative computer-aided approach to three-dimensional cephalometry and craniofacial imaging.

2. SPECIFIC AIMS

Specific aim #1. Development of Gold Standard Reference.

To calibrate and determine the accuracy and error uncertainty in three dimensions of the project test conditions, by developing a reference system to perform statistical comparisons of accuracy. The goals of the first step of validation are :

(i) Comparison of the measurement results between imaging modalities and the actual measurements of a pure rigid body (e.g. box, skull) and quantifying the absolute error.

(ii) Determination of the random and systemic measurement error of the imaging system when performed on a variable and complex craniofacial body (e.g. skull).

Specific aim #2. Determine Three-dimensional Calibration Evaluation.

Characterization of system generated three-dimensional spatial coordinates of box and skull landmarks attained through use of multiplane cephalometric and photographic images, which yield a three-dimensional mathematical map of selected landmarks and relationships.

Specific aim #3. Statistical Comparison of Measuring Modalities.

Statistically compare the computer generated three-dimensional linear distances generated by Sculptor™ to the gold standard developed from specific aim #1.

3. NULL HYPOTHESIS

The null hypothesis tested was that the three-dimensional linear measurements generated by Sculptor™ do not correlate with the true three-dimensional spatial relationships of craniofacial anatomic landmarks.

II. DESIGN

This investigation was primarily a validity and reliability study in which the accuracy and precision of a computer-aided three-dimensional approach to craniofacial imaging were evaluated. The experimental design and methodology used to accomplished the specific aims outlined in the introduction were as follows:

Specific aim #1: Development of Gold Standard Reference.

(i). Four plastic cubes of varying sizes ranging from 100 mm per side to 207 mm per side had 3 mm diameter metal bearings placed on each of the eight vertices.

(ii). The 28 distances between pairs of bearings on each object were determined by manual measurement utilizing a digital caliper (accuracy 0.03 mm). Each of four cubes were measured through five sessions of physical measurements, giving a total of 560 physical measurements.

(iii). Similarly, three plastic human skulls had a total of 40 skeletal and dental landmarks identified with metal bearings and subsequently surveyed using a digital caliper. Each of three skulls were measured through five sessions of physical measurements, giving a total of 940 physical measurements.

Specific aim #2: Calibration Evaluation.

Each object was placed additionally through an *imaging session*. Each imaging session consisted of a radiographic and photographic examination. The radiographic examination included three views acquired at different projection angles. The photographic session produced three or five recordings of all bearings. This required a minimum of three or five views at

different projections. During all of the imaging sessions, a calibration tool or frame was included in the field of view. This calibration frame is a rigid body with several fixed surveyed points whose three-dimensional spatial positions are known. This allows for automatic adjustment, or correction, through mathematical algorithms, for any distortion or magnification which takes place as these calibrated points are processed through the imaging session. One imaging session was then processed through a *system session* consisting of calibration of reference points, triangulation identification of selected landmarks, and computer-assisted measurements of distances between two landmarks. Five system sessions were performed on each image session to obtain five sampled measurements per distance.

Specific aim #3: Comparison of Measuring Modalities.

Statistical comparison of these assessments to the gold standard measurements derived from specific aim #1. This included a two-way ANOVA without replication statistical test.

III. MATERIALS AND METHODS

A. DEVELOPMENT OF STANDARD REFERENCE

1. RATIONALE

A rigid body has fixed points with fixed distances which can be measured with a high degree of precision. If measured with a highly accurate and precise instrument, the true three-dimensional relationship of preselected fixed points can be known. This is the principle rationale for developing a standard in which certain parameters (i.e. three-dimensional distances between two points) is known, verified, and, subsequently used as a gold standard. The Sculptor™ software has a unique self-calibration tool which requires use of a calibration frame placed on a subject. Certainly, this introduces a potential variable for error as the calibration frame is a separate object capable of movement on the patient's head. If we are to evaluate the error of the Sculptor™ imaging system alone, this variable of movement must be controlled for, by having some of the fixed metallic markers serve as the calibration tool. These markers can then function simultaneously as both calibration markers and points to be measured with the system. Once the error of the system is identified using this method, the error of applying the system to a more clinical application, such as skulls or live patients, may be evaluated and compared.

2 . TEST OBJECTS

The primary solid test objects used in this study were four plastic boxes and three plastic human skulls. Prior to testing the objects, each solid test object had a 3 mm radiopaque shotshell placed at each of the eight vertices on a given box or on a skull landmark (Table 1) to serve as a target that present

high contrast to both a closed captured device (CCD) video camera (Kodak, DC120 Zoom D.C., Eastman, N.Y.) and an X-ray image. A #8 carbide roundbur was used to drill a hemisphere at the vertices of these boxes or at the specific skeletal or dental landmarks on the skulls (Table 1), slightly less then half the diameter of a shotshell, and radiopaque markers were then fixed permanently onto these locations with superglue.

The boxes were labeled A, B, C, or D, with the top surface labeled by the respective letter, and the bottom surface labeled by the respective letter primed such as A', B', C', and D'. Each of the remaining four vertical faces were then labeled 1, 2, 3, and 4 following its corresponding box label (e.g., B2). Since a given vertex is constructed by the mergence of three planes, each vertex was labeled by the three planes which form it (e.g., B'B2B3).

Additionally, three plastic human skulls approximating the average actual size of a human skull were used as solid test objects. These were labeled A, B, and C. Landmark locations for the placement of the metallic markers were selected using defined criteria for each skull (Table 1). Skull A received 10 landmarks (i.e. craniosutural vertices and facial prominences). Skull B had 15 common skeletal anatomic reference landmarks used in traditional two-dimensional cephalometrics [7]. These included both midsagittal and bilateral landmarks. Skull C was used to depict 12 dental landmarks; specifically apical points of maxillary and mandibular right and left first molars, the mesial buccal cusps of maxillary and mandibular right and left first molars, the apex and incisal edges of the left maxillary and mandibular central incisors, and three frontal skeletal landmarks. 40 landmarks were used with only three overlapping landmarks on different skulls. A descriptive list of all 37 different landmarks is provided in Table 1.

3. PHYSICAL MEASUREMENTS

Surveying of the test object targets was necessary for the calibration evaluation of the cubes and skulls, so that a calibration evaluation of the video camera and X-ray imaging sensor could subsequently be performed. The linear distances between the metallic markers of all test boxes A, B, C, D and skulls A, B. and C were measured. The distance between pairs of bearings or landmarks on each object was determined by manual measurement utilizing a digital caliper with accuracy equal to 0.03 mm, according to the manufacturer. For the cubes, one measuring session consisted of measuring twenty eight distances between pairs of markers on each of four cubes. Each session was repeated four more times giving a total of five sessions of physical measurements. This resulted in a total of 560 physical measurements on the cubes alone. Similarly for the skulls, one measuring session consisted of measuring 45, 69, and 74 measurements for skulls A, B, and C, respectively. Each session was repeated four more times giving a total of five sessions of physical measurements. This resulted in a total of 940 physical measurements on the skulls. Therefore the total number of physical measurements alone (excluding the system measurements) in this study were 1500 total physical measurements.

The mean distance, standard deviation and error associated with each of the 1500 measurements were calculated (intraoperator reliability). From these data, a reproducibility margin (intraclass correlation) of 0.999996 (with 1 being perfect) was calculated using a 2-way ANOVA test for the cubes. This was equivalent to a measurement error of 0.085 mm.

For the skulls, an intraclass correlation of 0.999992 and a measurement error of 0.095 mm was calculated using the same statistical test.

Table 1. Definition of Skull Landmarks

1. Bregma (Bgma) -point of junction between the right and left coronal sutures and the sigittal sututre.

2. Corona Left (Crna L) - point of junction between the left coronal, and left frontoethmoidal sutures.

3. Corona Right (Crna R) - point of junction between the right coronal, and right frontoethmoidal sutures.

4. Glabella (G) - the most prominent point in the midsagittal plane of the forehead.

5. Zygoma Left (Zyg L) - point of junction between left zygomatic and left temporal b bone.

6. Zygoma Right (Zyg R) - point of junction between right zygomatic and right temporal bone.

7. Mastoid Left (Mas L) - most anteroinferior point of left mastoid process.

8. Mastoid Right (Mas R) - most anteroinferior point of right mastoid process.

9. Anterior nasal spine (ANS) - tip of the bony anterior spine in the midsagittal plane.

10. Gnathion (Gn) - the most anteroinferior point on the symphysis in the midsagittal plane.

11. Posterior clinoid (P Clin) - the point representing the posterior midpoint of the posterior clinoid.

12. Nasion (N) - the most anterior point of the frontonasal suture in the median plane

13. Orbitale (Orb L) - the lowest point in the inferior margin of the left orbit.

14. Orbitale Right (Orb R) - the lowest point in the inferior margin of the right orbit.

15. A Point (A) - the deepest midline concavity on the maxilla between ANS and prosthion.

16. Condylion Left (Co L) - the most central point on the left condylar head.

17. Condylion Right (Co R) - the most central point on the right condylar head.

18. Porion Left (Po L) - the most superoposterior point of the lef temporomandibular fossa.

19. Porion Right (Po R) - the most superoposterior point of the right temporomandibular fossa.

20. B Point (B) - the deepest midline concavity on the mandibular symphysis between pogonion and infradentale.

21. Gonion Left (Go L) - the point of intersection between the left ramal plane and the left mandibular plane

22. Gonion Right (Go R) - the point of intersection between the left ramal plane and the left mandibular plane

23. Posterior nasal spine (PNS) - tip of bony posterior spine in the midsagittal plane.

24. Frontozygoma Left (Fz L) - the point of junction between the left frontal bone and the left zygomatic bone.

25. Frontozygoma Right (Fz R) - the point of junction between the left frontal bone and the left zygomatic bone.

26. UL1A - point corresponding to upper left central incisor apex.

27. UL1I - point corresponding to upper left central incisor incision.

28. LL1A- point corresponding to lower left central incisor apex.

29. LL1I - point corresponding to lower left central incisor incision.

30. UL6A - point corresponding to upper left first molar apex.

31. UL6MB - point corresponding to upper left first molar mesiobuccal cusp.

32. LL6A - point corresponding to lower left first molar apex.

33. LL6MB - point corresponding to lower left first molar mesiobuccal cusp.

34. UR6A - point corresponding to upper right first molar apex.

35. UR6MB - point corresponding to upper right first molar mesiobuccal cusp.

36. LR6A - point corresponding to lower right first molar apex.

37. LR6MB - point corresponding to lower right first molar mesiobuccal cusp.

B. IMAGING AND PROCESSING

1. IMAGE ACQUISITION

Each object (boxes A ,B, C, and D and skulls A, B, and C) was used in five imaging sessions. Each imaging series consisted of a radiographic and photographic examination. The radiographic examination included three views acquired at different projection angles. For the boxes, the photographic session produced three recordings of all eight bearings, acquired from multiplanar views. This required a minimum of three views at different projections. As previously mentioned, during all of the imaging series, the fixed metal bearings may purposefully serve as a calibration tool or frame when included in the field of view.

For the skulls, a special propriety calibration framework designed specifically for patient use by Acuscape Corporation (Quail Ridge Center, 1200 East Alosta Ave, Glendora, Ca, 91740) was placed on the skulls for the imaging series. An imaging series consisted of three multiplanar radiographic images taken at different, but consistent views, and five multiplanar digital photographic images taken at different but consistent views as well. All imaging series and sessions were taken by a single calibrated and trained technician. The calibration framework was not replaced between imaging series for each skull and care was taken not to move its position relative to the skull.

2. IMAGE PROCESSING[30]

The Sculptor™ technology and software allows accurate three-dimensional modeling of hard and soft tissue anatomical landmarks from multiple cephalometric films and photographs. Sculptor™, which is the software developed as a result of this technology, combines modern digital

photogrammetry with image analysis in a workstation environment based on Windows PC software. A unique self-calibration feature of the software, based on advanced digital imaging and photogrammetry algorithms, eliminates the need for object/subject fixation mechanism of a cephalostat while compensating for all magnification and rotation effects. This calibration technique further allows geometric cross-calibration of the visible band images such as digital color photographs and video frames with the scanned radiographic (cephalometric) films. This provides the capability to superimpose three-dimensional hard tissue landmarks and traces onto digital photographs or captured video frames with accurate registration to the photographic view.

Sculptor™ uses existing low-cost x-ray imaging equipment, standard flatbed scanners, and runs on the Windows PC platform. Its graphical user interface controls the analytic functions via user inputs. The on-line analysis results are graphically displayed for confirmation and editing on multiple image windows. The relational database behind the software keeps track of the anatomical structures, images, three-dimensional landmark co-ordinates, and calibration data in a unified framework.

The cephalometric films are scanned at 6 pixels per mm and stored using JPEG compression without any noticeable degradation. The resulting storage requirements are about 150 Kbytes per film. Scanners with 10-bit gray scale resolution that are optimally mapped to eight bits, produce better coverage of the large range of densities usually found in cephalometric films.

The submillimeter predicted accuracy of Sculptor™ is achieved by systematically addressing the error sources in the process. As in any photogrammetric triangulation process, the final deviation from physical truth results from a combination of several error sources. Some of these

errors are inherent to the image sensor resolution and noise which can be considered fixed and are determined off-line. However, a more important set of these parameters depend on the geometry and size of the very object being measured. Based on these factors, theoretical error bounds can be internally computed from calibration data, camera resolution, and other system parameters for a specific measurement scenario. The technology behind Sculptor™ includes the necessary models and algorithms to compute these theoretic error bounds and present them as part of the measurement results. For example, for each measured landmark, the software computes the ellipsoid that represents the error uncertainty in three dimensions. In this way the user is given a yard stick by which the accuracy of each measurement can be judged.

In the case of cephalometric landmark measurements, submillimeter accuracy was predicted and experimentally validated by exercising these analytic error models. This occurred with the assumption that no gross landmark association error has resulted. Since the association error is minimized by the unique approach used in Sculptor™, we can claim this accuracy to be valid.

Locating a feature in each view can be accurate to a small fraction of a pixel by using automated feature-finding and tracking tools. At the same time, the calibration procedure incorporated in Sculptor™ reduces the measurement bias to submillimeter values. An important error source, however, arises from wrong association of landmarks and structures in two or more radiographic views of the skull for the purpose of triangulation. Due to the nature of X-ray imaging, this association is more difficult for radiographs than photographs. On the other hand, the accurate geometric calibration of Sculptor™ causes the landmark association in different views

to be simplified. The accurate calibration provides an instant cross-checking capability and avoids gross-association errors. To a large extent, this cross-checking function has been automated in Sculptor™.

An accurate geometric calibration creates an epipolar line corresponding to a point in an image on a second image of that point. Therefore, the associated point in the second image can lie only on the epipolar line. To increase the accuracy, or to reduce the ellipsoid of error uncertainty even more, a third calibrated image can be incorporated to the calibration session to further reduce the association error by identifying the same corresponding point. The reverse relationship is also true and can be used for further confirmation. In addition to point landmarks, an important use of this basic property is that extended landmarks such as orbital rims and mandibular canal can be associated easily once the epipolar constraint is quantified. An example of how this is achieved is shown in Figure 1 where two cephalometric images of a dry skull are processed by Sculptor™ to obtain three-dimensional traces for the right and left halves of the mandible. Figure 1 shows the tracing of the right half of the mandible in the images and the epipolar lines drawn in one image corresponding to points on the trace in the other image. These lines are used to establish the corresponding point pairs from two traces that are used for triangulation.

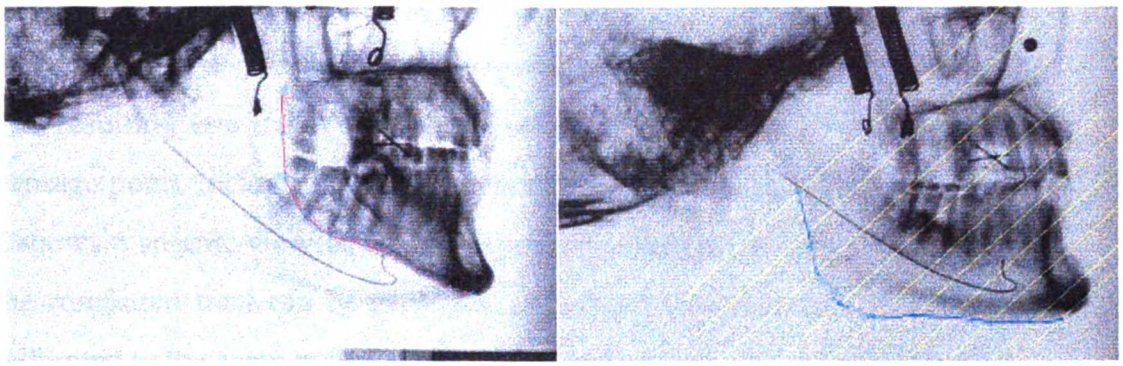

Figure 1. Sculptor™ tracing of right half of mandible on oblique view and epipolar line corrsponding to lateral view.

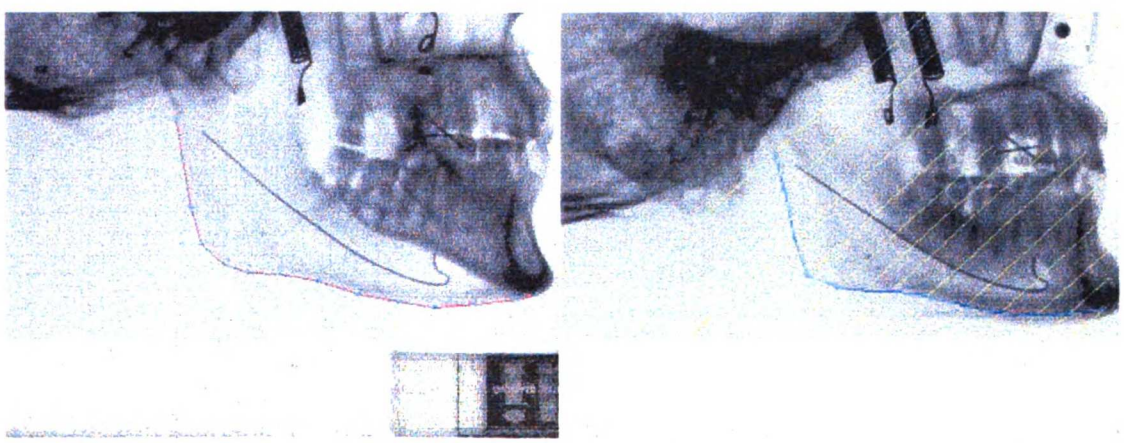

Figure 2. Sculptor™ tracing of left half of mandible on lateral view and epipolar line corrsponding to oblique view.

Once the point pairs and their corresponding three-dimensional coordinates are found, a trace is formed in three-dimensions by connecting the points.

Figure 2 shows this process repeated for the left half of the mandible. The resulting two traces can now be viewed by Sculptor™ from any virtual vantage point, including photographic rather than radiographic views. Figure 3 shows a specific view of the two traces. To confirm and/or edit the result, the computed trace can be projected on a third cephalometric image that is calibrated to the same measurement coordinates. This is shown in Figure 4

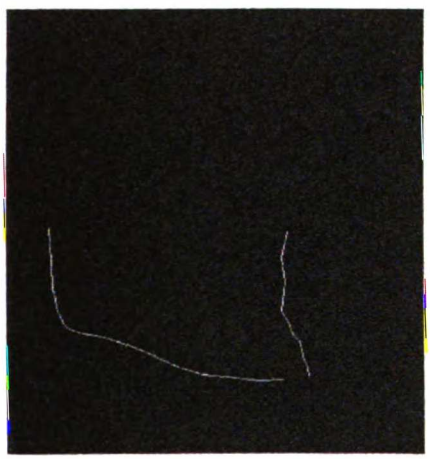

Figure 3. Specific different view of same tracing

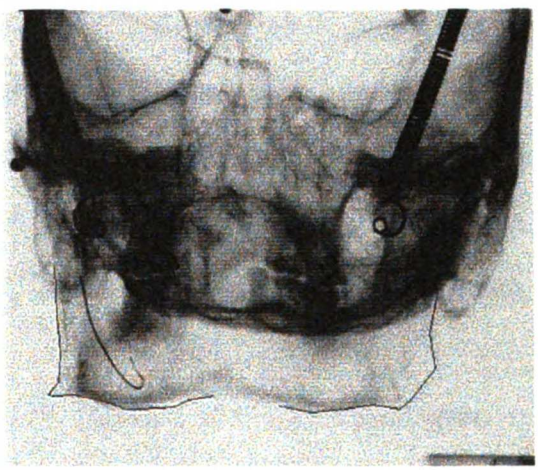

Figure 4. Computed tracing projected on third cephalometric image.

which is a view roughly 90 degrees from the two views used to obtain the traces. The projection shows that, except for one possible missed point, the traces accurately project onto the corresponding structures in the third view.

Once we know that chances of an association error have been removed, accurate geometric calibration allows us to claim the accuracy predicted by the analytic model. For the nominal condition of the X-ray imaging geometry and calibration frame used in this experiment, the computed accuracy was defined with an error ellipsoid with dispersion of 0.5 millimeter or less in three-dimensions.

3. SOME DETAILS OF ANALYTIC ACCURACY MODEL[30]

The analytic model for triangulation accuracy takes all error sources except the association error into account by propagating and combining the error covariance of various parameter errors through the photogrammetric projection and triangulation functions. The result is the error covariance of the position of three-dimensional coordinates of the landmarks. The sources of error include those arising from errors in locating a feature in the image space and the calibration errors associated with the following calibration procedures:

(i) Interior orientation calibrations parameters of the imaging system, which in the case-scanned-cephalometric-films are: Source-to-film perpendicular distance, scanning resolution of the film in pixels per millimeter, and the location of the center of projection in pixel coordinates.

(ii) Exterior orientation calibration parameters of the imaging system for each cephalometric film taken, namely: position and orientation of the measurement coordinate system attached to the skull relative to

the film-source coordinate system. This is estimated as six degrees of freedom (i.e., roll, pitch, yaw, X°, Y°, Z°) of the skull coordinate system relative to the sensor coordinate system.

(iii) The values for these calibration parameters were estimated in accuracy experiments which compared the cephalometric imaging modality with stereo video triangulation results. The 0.5 mm accuracy predicted and verified by the model was based on the conservative assumption of locating features in the pixel domain to be within 2.5 pixels as the standard deviation error.

The Acuscape core technology provides the ability to render a composite three-dimensional image by fusing photographs or visual light images with the three-dimensional skeleton rendered from cephalometric images and the system cross-calibrates both image sets to a common coordinate system. A digital replica (e.g., an accurate three-dimensional computer duplication) of the maxillomandibular complex can be created by the extraction of selected landmark locations from the cross-calibrated cephalometric and tomographic images using the Sculptor™ software. The following is an illustration of a digital replica that was rendered with Acuscape technology. In figure 5a, a skull was photographed at two different angles. From these photographs, a wireframe (figure 5b) and a phototextured (figure 5c) model of the skull was rendered. Figure 5d are three dimensional digital replicas of the original skull. The digital replicas can be rotated to any vertical angle for viewing, landmark identification, measurement, or analysis.

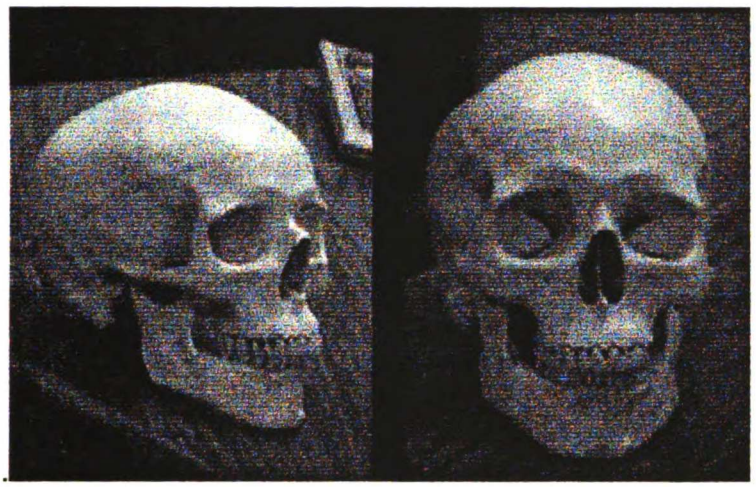

Figure 5a

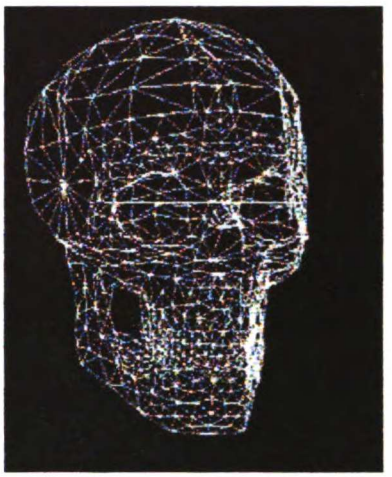

Figure 5b

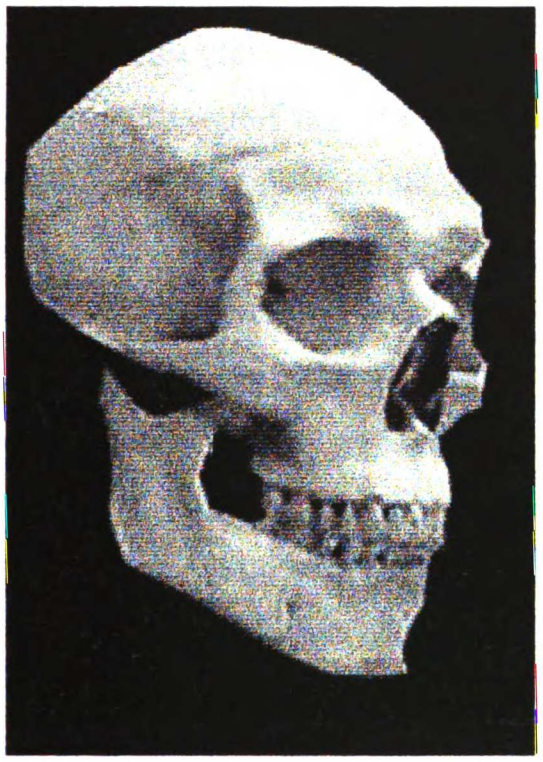

Figure 5c

Figure 5d

Figure 5. Rendering process of digital skull replica by Sculptor™. a) Skull ph≥≥otogrpahed at two different angles. b) Wireframe model of skull calculated by Sculptor™. c) Phototextured model of skull rendered by Sculptor™. d) Versatility of replica manipulation showing change of size or viewing angle.

4. 3-D DISPLAY[30]

The purpose is then to display in three dimensions, all of the multiplanar images need to be registered on a common coordinate system using a reference plane or calibration frame. The reference plane is created with external markers that are imaged along with the objects/subjects anatomy. It merges two or more cephalometric-type head films acquired at approximately prescribed head orientations into a single accurate three-dimensional database of anatomical structures. The computed traces and landmarks are displayed in virtual view with the ability to interactively change the viewing angle.

C. CALIBRATION EVALUATION

This effort concentrated on validating the achievable accuracy and identification of the random and systematic errors of the three-dimensional computer-aided approach. The accuracy and precision of the system to be evaluated depends on the accuracy and precision of two important computer-user interface processes: calibration and triangulation. First, the problem of calibration of reference markers from the calibration frame onto a common coordinate system, requires computer-aided accurate marker identification of these control points on multiple images. Second, the problem of landmark registration requires computer-assisted accurate triangulation of landmark identification from multiple views.

Recall that each image session consisted of six views for the cubes (three radiographic and three photographic) and eight views for the skulls (three radiographic and five photographic). Each image session was then put through a system session which consisted of two parts: calibration of all six or eight images from an image session and triangulation of landmark

identification using at least three views. The three-dimensional spatial coordinates of all landmarks were, thus, automatically and mathematically registered in the system's data base. At this point, determination of any three-dimensional linear distance between any two previously identified was automatic. Each system session for each image session was repeated four times to give a total of five measurement sessions or five measurements per distance. Like the physical measurement of the test objects, 875 computer-aided measurements from the radiographic images and 430 computer-aided measurements from the photographic images were obtained.

D. STATISTICAL EVALUATION

Data were evaluated by two approaches. First, the physical measurements of the calibration equipment was expressed in mean values with both standard deviation to assess sample variation and standard error to evaluate the difference of mean values. Data obtained from multiplane radiographic, or photographic images (Sculptor™ recordings) were compared to physical measurements. The Sculptor™ recordings were statistically compared with the physically measured gold standard and coordinate differentials were derived. A standard ANOVA test was used to test whether the digital radiographic and digital photographic Sculptor™ readings and the physically generated coordinates were from the same population or not.

Additionally, a 2-way ANOVA test without replication was performed to evaluate the similarity coefficient of the three samples (physical, radiographic, and photographic measurements). From this a reproducibility margin, an intraclass correlation value was calculated.

IV. RESULTS

A. REFERENCE PHYSICAL MEASUREMENTS

1. BOXES

A total of 560 physical measurements between marker vertices on boxes A, B, C, and D were performed. Each box contained 28 possible measurable distances which were surveyed five times with precision digital calipers. The surveyed mean values and corresponding variances of each location distance are presented in Tables 2 and 3.

In order to determine the reliability of individual measurements and to assess the level of observer variability, an analysis of variance model was used to characterize session measurement variability. This test gives a mathematical value of the degree of similarity between measurements which reflects the usefulness of this model to serve as a reference gold standard and by which the remaining experiments may be completed[37].

A 2 way ANOVA without replication for the box measurements was performed to arrive at an intraclass correlation value of 0.999996, with a value of one indicating perfect agreement. Note the submillimetric variance of all location measurements in Tables 2 and 3, which range of 0.169 mm (maximum) to 0.00012 mm (minimum) and a mean variance of 0.0085 mm. The standard deviation, which is an indication of the overall variability of these sessions, was 0.086 mm. The standard error of the mean, which quantifies the precision of these estimates, was 0.0073 mm^2 .[37, 38]

It was of interest to know if there was a tendency for the larger mean distances to have greater variation. In an effort to determine if there was a direct relationship between the variation of measurements and the mean distances, a linear regression was performed. Figure 6 demonstrates that

there is no relationship between mean distance and variation. Minimal variation was uniformly found throughout the entire spectrum of mean distances.

2. SKULLS

A total of 940 physical measurements between landmark markers on skulls A, B, and C were performed. Skulls A, B, and, C contained 45, 69, and 74 possible measurable distances, respectively, which were surveyed five times with precision digital calipers. Since the Sculptor™ program automatically calculates the centroid of a spherical marker when calculating its three-dimensional coordinates, but since the physical measurement were measured as the maximum distance between two markers and not the centroid, it was necessary to factor, or subtract the radius of each of the two metallic markers during all physical measurements. This adjustment factor was taken as the mean diameter of 35 metallic markers randomly selected from the same batch of markers as used on the test objects. This adjustment value was 2.758 mm, with a range of 0.40 mm. The adjusted mean values and corresponding variances of each location distance are presented in Tables 4, 5 and 6.

The same statistical analysis test as above was performed to evaluate the repeatability and intraclass correlation of the repeated physical measurements between landmark locations on all three skulls. The intraclass correlation value for the three skull physical measurements was equally consistent with a value of 0.999992, with a value of one being perfect. Tables 4 through 6 list the adjusted mean values with the associated variances. The calculated standard deviation of the means was 0.095 mm. The standard error of the mean, was 0.009062 mm^2.

The magnitude of error for either the box or skull physical measurements are virtually null with respect to the range of the dimensions being measured (6 mm - 207 mm). Therefore, the values provided in Tables 2 - 6 are taken to be the gold standard values against which the accuracy of a digital imaging system capable of determining linear distances between two points in three dimensions of space may be compared to.

Figure 7 demonstrates a lack of relationship between the variance and the mean distances for the physical measurements performed on the skulls.

B. DIGITAL RADIOGRAPHIC MEASUREMENTS

1. BOXES

A digital calibration frame for the boxes could not be provided for by Acuscape Corp. prior to the completion of this portion of the study. Therefore, it was not possible to assess the accuracy and precision of digital radiographic determined three-dimensional linear distances on the box solid test objects. However, this study has produced five digital radiographic sessions of all four boxes consisting of three multiplanar views each and has effectively produced a validated gold standard of its physical dimensions in three planes of space, by which to measure such digital photographic measuring capabilities, once this digital calibration frame becomes available in the future. These gold standard values are provided in Tables 2 and 3 for future testing and calibration purposes.

2. SKULLS

A digital calibration frame for the skulls was kindly provided for by Acuscape Corp., which made three-dimensional linear measurements possible from digital radiographic images. Most physical measurements

performed on the skulls were repeated using the Sculptor™ program to give a total of five measurement session per location. A total of 875 digital radiographic three-dimensional measurements were performed collectively on skulls A, B, and C. The mean values and associated variances are presented in Tables 7, 8, and 9. The landmark Bregma was not identifiable on all three multiplanar radiographic views, therefore, all locations which included this landmark were omitted from the experiment. Similarly, the dental landmark LR6MB (see Table 1) did not have a digital entry prompt as it was accidentally left out during the programming of landmark listings for Sculptor™. Therefore, all locations which included LR6MB were also omitted from this study. Additionally, the location Corona left to Corona right had a variance of 0 measured to a millionth of a millimeter (e.g. 118.880378 mm) after five sessions, which presents as a highly questionable physical possibility and remains as an unexplained error, and thus, was also omitted from the final comparisons in the later portions of this study.

The mean variance for skull A was 0.027 mm, for skull B the variance was 0.14 mm, and for skull C the variance was 0.064 mm. The total variance for all skulls was 0.09 mm in terms of the digital radiographic three-dimensional linear measurements

The intraclass correlation for the digital radiographic measurements was calculated to be 0.999969, again with a value of one being perfect. The associated standard error of the mean was equal to 0.0262 mm^2 and the standard deviation was 0.1620 mm, as per the 2-way ANOVA test. Thus, the precision of the Sculptor™ program for the radiographic determination of a landmark's three-dimensional position was equivalent to 0.0262 $mm^{2,}$, which is an extraordinary level of precision, or repeatability, by any standard.

There was no detectable relationship present between increasing mean distances measured radiographically and the variance of the measurements, as shown in figure 8.

C. DIGITAL PHOTOGRAPHIC MEASUREMENTS

1. BOXES

A digital calibration frame for the boxes could not be provided for by Acuscape Corp. prior to the completion of this portion of the study. Therefore, it was not possible to assess the accuracy and precision of digital photographic determined three-dimensional linear distances on the box solid test objects. However, this study has produced five digital radiographic sessions of all four boxes consisting of three multiplanar views each and has effectively produced a validated gold standard of its physical dimensions in three planes of space, by which to measure such digital photographic measuring capabilities, once this digital calibration frame becomes available in the future. These gold standard values are provided in Tables 2 and 3 for future testing and calibration purposes.

2. SKULLS

A digital calibration frame for the skulls was also kindly provided for by Acuscape Corp., which made three-dimensional linear measurements possible from digital photographic images. Close to half of the measurements made physically on the skulls were repeated using the Sculptor™ program, to give a total of five measurement session, per location. A total of 430 digital photographic three-dimensional measurements were performed collectively on skulls A, B, and, C. The mean values and associated variances are presented in Tables 10, 11, and, 12. Many of the landmarks were not

identifiable on all three multiplanar photographic views, mostly because the calibration frame covered theses landmarks and impeded their visual identification. Most of the landmarks which were covered by the calibration frame were from skull A. Therefore, all locations which included these landmark were also omitted from the experiment.

The mean variance for skull A was 0.167 mm, for skull B the variance was 0.152 mm, and for skull C the variance was 0.060 mm. The total variance for all skulls was 0.097 in terms of the digital radiographic 3-D linear measurements.

The intraclass correlation for the digital radiographic measurements was calculated to be 0.999939, the associated mean standard error was 0.054 mm^2, and the standard deviation was 0.232 mm, as per the 2-way ANOVA test. The submillimetric precision of the Sculptor™ program during this portion of this investigation was determined to be equivalent to 0.054 mm^2.

As with the other measuring modalities, there was no detectable relationship between the variance and the mean distances, as determined by the photographic measurements (figure 9).

D. COMPARISON OF MEASUREMENTS

Tables 13, 14 and 15 present the comparison of the Sculptor™ digital three-dimensional measurements with the gold standard measurements derived from Tables 4,5 and, 6. Since the digital photographic measurements only totaled 430 with 86 mean values (430 measurements/5 sessions) , the number of possible comparisons was limited to 86. Of these the majority of comparisons were from Skull C. A 2-way ANOVA was performed to evaluate the degree of similarity between the three different measuring modalities (i.e., physical vs. digital radiographic vs. digital photographic) and

to test the null hypothesis that the three-dimensional linear measurements generated by Sculptor™ are not the same as the gold standard measurements.

The results of the 2-way ANOVA indicated an intraclass correlation of 0.999952, with a value of one representing perfect agreement among measuring modalities. The standard error of the mean was calculated to be 0.0379 mm^2, and the standard deviation was 0.195 mm. There was no statistically significant difference between the three-dimensional linear radiographic and photographic measurements generated by Sculptor™, and the gold standard measurements. The level of significance was tested at $P < 4.65X10^{-9}$. This means the chance that the three measurement values (i.e., physical vs. digital radiographic vs. digital photographic) were different but that the difference wasn't detected, was less than 0.000000465%.

Since the analysis of variance statistical test yielded nonsignificance for the three different measuring modalities, it was not necessary to test for individual statistical difference among measuring modalities. However, it is necessary to compare the mean differences between measuring modalities in order to calculate the accuracy with which Sculptor™ determines the three-dimensional linear distance between two points in space.

Tables 16, 17, and, 18 present the difference between the Sculptor™ digital radiographic three-dimensional measurements and the gold standard measurements for Skulls A, B, and, C, respectively. The difference was taken as the absolute difference in all cases, so as not to average out the magnitudes of the difference which would have given an erroneous representation of the error. The mean difference of the error (n=170) between the Sculptor™ digital radiographic three-dimensional measurements and the gold standard measurements was 0.221 mm, with a range of 0.871 mm and a standard deviation of 0.175 mm. Recall that the range of the physical measurements

of the metallic markers was 0.40 mm, when measuring the radius of two markers. It was necessary to account for this range at this point. Therefore, the adjusted and actual range of the Sculptor™ system is 0.471 mm for digital radiographic measurements, and the average accuracy was equivalent to 0.221 mm. However, there were certain differences in accuracy between skulls. For instance Skull B (n=69) had the least accuracy at 0.264 mm, while Skull C (n=66) showed the highest level of accuracy at 0.173 mm. This was a measure of the accuracy of the Sculptor™ system, or its ability to accurately determine the three-dimensional position of a skull landmark using digital radiographs in a controlled setting.

Similarly, Tables 19, 20, and, 21 present the difference between the Sculptor™ digital photographic three-dimensional measurements and the gold standard measurements. The mean difference of the error (n=86) between the Sculptor™ digital radiographic three-dimensional measurements and the gold standard measurements was 0.253 mm, with an adjusted range of 0.737 mm and a standard deviation of 0.212 mm. Skull A presented the least level of accuracy at 0.452 mm, and again, Skull C presented the highest level of accuracy at 0.198 mm. This is a numerical expression of the ability of the Sculptor™ system to accurately determine the three-dimensional position of a skull landmark using digital photographs in a controlled setting.

Comparison between the Sculptor™ digital photographic and radiographic three-dimensional measurements are presented in Tables 22, 23, and, 24, for Skulls A, B, and, C, respectively. The mean difference between the two digital measuring systems was 0.221 mm, with a range of 0.471 mm. Skull C presented the least mean difference at 0.172 mm.

Finally, to graphically demonstrate the relationship of agreement between the physical measurements and the digital measuring modalities, a linear regression was performed. Figures 10 and 11 show a near perfect direct relationship between the physical measurements and the radiographic and photographic measurements, respectively.

V. DISCUSSION

A. VALIDATED GOLD STANDARD

One of the specific aims of this investigation was to develop a gold standard with which to evaluate the accuracy of a computer-aided approach to three-dimensional craniofacial imaging. This involved determining the true three-dimensional linear distances between fixed points of test objects (e.g., boxes and skulls), with a high degree of precision, by surveying these points with a digital caliper of high accuracy (0.03 mm).

Measuring the distances between test points was necessary for the calibration evaluation of the cubes and skulls, so that a calibration evaluation of the digital camera and X-ray three-dimensional measurement modalities could subsequently be performed. A total of 300 distances on the boxes and skulls were measured five times to give a total of 1500 physical measurements. The repeatability, reproducibility, or precision of these repeated measurements were determined using a 2-way ANOVA statistical test. A correlation coefficient indicating the degree of agreement between measures was calculated to be 0.999996 and 0.999992 for the boxes and skulls, respectively. The maximum possible value for a correlation coefficient is one, indicating perfect agreement. The mean standard deviations, the overall variability, were 0.086 mm and 0.095 mm, for the boxes and skulls, respectively. The standard error of the means, which quantifies the precision of these estimates, was 0.0073 mm^2 and 0.009062 mm^2, for the boxes and skulls, respectively. Therefore, these values were taken to be sufficiently consistent in terms of precision, to serve as references with which to validate the Sculptor™ system accuracy. The surveyed distances, and their respective variances, are presented as gold standard values in Tables 2 through 6.

B. ACCURACY AND PRECISION OF A THREE-DIMENSIONAL APPROACH

This effort concentrated on validating the achievable accuracy of the three-dimensional computer-aided approach. A three-dimensional coordinate system was derived for each cube and skull and the (x,y,z) location of each of the metal bearings was determined from the imaging modalities and statistically compared to the manual/physical measurements.

The accuracy and precision of the system to be evaluated depends on the accuracy and precision of two important computer-user interface processes: calibration and triangulation. Most of the error in the system is attributable to one, or both, of these processes. First, the problem of calibration of reference markers from the calibration frame onto a common coordinate system requires computer-aided accurate marker identification of these control points on multiple images. Second, the problem of landmark registration requires computer-assisted accurate triangulation of landmark identification from multiple views.

Recall that each image session consisted of six views for the cubes (three radiographic and three photographic) and eight views for the skulls (three radiographic and five photographic). Each image session was then put through a system session which consisted of two parts: calibration of all six or eight images from an image session and triangulation of landmark identification using at least three views. The three-dimensional spatial coordinates of all landmarks were automatically and mathematically registered in the system's data base. At this point, determination of any three-dimensional linear distances between any two previously identified points was automatic. Each system session for each image session was repeated four

times to give a total of five measurement sessions or five measurements per distance.

The precision, or measure of repeatability, of the radiographically determined three-dimensional linear measurements was 0.0262 mm^2. For the photographically determined three-dimensional linear measurements, the precision was 0.054 mm^2. Thus the consistency of the Sculptor™ system appears to be well within the demands for clinical usefulness, and far superior to any traditional cephalometric landmark identification approach presented thus far. .

The accuracy, or "truthfulness" of measurement, of the Sculptor™ system was 0.221 mm for the radiographic determinations, and 0.253 mm for the photographic determinations. However, the achievable accuracy of the Sculptor™ system under highly controlled settings of image acquisition, calibration and triangulation, was in the order of 0.173 mm and 0.198 mm, for the digital radiographic and photographic sessions, respectively. These were the accuracy levels which were consistently obtained in Skull C.

Skull C may have had a greater level of accuracy due to several reasons. First, during the system sessions, it was evident that calibration and triangulation occurred with the greatest ease in all five skull C system sessions compared to skulls A and B, indicating that the system error was the least for these sessions. Second, ease of calibration and triangulation is directly dependent on the image acquisition process of not allowing the calibration frame to move during the imaging sessions. It is highly likely, that the framework on skull C experienced the least movement of all skulls, and hence experienced a greater accuracy of calibration and triangulation. Finally, all skulls were measured in the sequence of A, B, and C. It is also likely , that since calibration and triangulation requires a certain degree of operator

training and experience, and since skull C was always the last to be measured either physically or digitally, that a small but significant difference in operator skill was consistently present during all skull C measurements.

C. SOURCES OF ERROR AND OTHER COMMENTS

Although submillimetric in nature, it is necessary to discuss potential sources of random and systematic errors of this three-dimensional computer-aided approach. The accuracy and precision of the system begins with the highly controlled image acquisition process, necessary for geometric cross-calibration of multiple views, from either visible band images or scanned radiographic films. The use of a unique self-calibration framework provides the capability to register the same point from different images, to a common coordinate three-dimensional database. The requirement, however, is that no movement of the calibration framework take place during the imaging process. Any movement of the framework during this process can alter the geometric relationship between the same points on various images. One of the assumptions of this experiment was that the test objects were rigid bodies. However, submillimetric flexure of these plastic bodies (e.g., boxes and skulls) was theoretically possible during the image acquisition process. Additionally, the skulls were not completely rigid, as they contained three moveable parts, mainly the cranial roof which was held by two hinge screws and the mandible which was held in place by one hinge screw on a stainless steel spring.

Another potential source of error is the inaccuracy of the physical measurements between the calibration points on the calibration framework itself. The accuracy of the Sculptor™ system depends on the accuracy of the calibrated framework device. Given the high degree of accuracy in these test

conditions, it is not likely that the calibration frame was measured inaccurately.

Finally, it is conceivable that the physical measurements were less accurate than the Sculptor™ system measurements. The physical measurements were not free of possible random or systematic errors, particularly since only one operator performed all physical measurements. Although the five measurement sessions were purposely performed on five different days, operator bias is likely when only one operator performs all measurements. Parallax error is always a potential source of error when measuring a linear distance with a straight-edge caliper. The metallic markers were fixed and coated with superglue, which automatically increases the marker diameter. This "glue factor" is highly variable and, thus, could not be accounted for systematically . Finally as mentioned above, all test objects were made of plastic material, susceptible to flexure and expansion depending on ambient conditions such as temperature, humidity, and atmospheric pressure.

Although each of these factors may seem insignificant by itself, collectively, they account for the mean 0.2 mm difference between measuring modalities.

D. SIGNIFICANCE AND FUTURE APPLICATIONS

A significant limitation of conventional imaging modalities in maxillofacial radiology has been the lack of practical, cost-effective methods to accurately represent anatomy. Craniofacial structures are three-dimensional in nature, and it has been difficult to identify a (three-dimensional) point in two or more projections acquired from different views [24, 28].

The tested system mathematically manipulates image data through the use of algorithms which perform various functions. Recent advances in computer hardware technology allow for such practical and convenient "soft copy" image exploitation [22].

A limitation of previous stereophotogrammetric approaches to three-dimensional cephalometrics has been the previously discussed "association error". This inaccuracy of identifying the same point on two or more images is proportional to the divergence of the angle between the two projections. Until recently, only CT scans offered a solution to this problem by sampling a large number of small angle increments around the object, after which any given "feature" is correctly located as a result of the mathematical image reconstruction process itself [22]. The financial cost and radiation exposure limits its use as a routine diagnostic tool.

Finally, as to date, the use of physical records has routinely allowed clinicians and researchers to assess changes and variability in craniofacial and dental morphology, individually. However, none of the physical records allow for a composite understanding of the sum of parts. For instance, information from one physical modality (i.e. study casts) is usually lost when examining another physical modality (i.e. headfilm), and so is the potential for integrating information from various forms. Digital anatomical mapping into three-dimensional coordinates, offers a solution to this historical problem, by allowing integration of information to a common coordinate system. Furthermore, this integration of data allows quantitation between records of various forms. The system evaluated herein, provides the technology and accuracy to accomplish this integration.

The applications in both research and clinical use are limited by one's imagination. Having a mathematical three-dimensional data base for

anatomic points obtained from digital images, and registering these points to a common coordinate system, can significantly expand and integrate data bases from the scientific community throughout the world. The technology appears to be available now, and the accuracy and precision of this method has been demonstrated in this study.

VI. CONCLUSIONS

The recent advent of digital technology has given new validity to traditional cephalometry by eliminating much of the error associated with image acquisition and landmark identification inherent in traditional cephalometric analysis, thus, allowing for highly accurate three-dimensional image acquisition.

The Sculptor^{TM} system combines digital technology with modern stereophotogrammetry, and includes a built-in calibration technique which automatically corrects for external errors. This system was evaluated for its claimed accuracy and precision. The results obtained include:

1) Successful development of a gold standard with which to evaluate the accuracy this computer aided approach to three-dimensional craniofacial imaging. The precision of the gold standard measurements were nearly perfect, with intraclass correlations of 0.999996 and 0.999992.
2) The mean values obtained from the gold standard measurements, and the Sculptor^{TM} system measurement were compared using a 2-way analysis of variance. There was no statistical difference between these three groups.
3) The *precision* with which the Sculptor^{TM} system can determine the three-dimensional spatial coordinates of an anatomic point in space, from digital radiographs is 0.0262 mm^2, and 0.054 mm^2, from digital photographs.
4) The *accuracy*, with which the Sculptor^{TM} system can determine the three-dimensional spatial coordinates of an anatomic point in space, from digital radiographs was 0.221 mm, and 0.253 mm, from digital photographs.

5) The *achievable* accuracy of the Sculptor^{TM} system under highly controlled settings of image acquisition, calibration and triangulation, was in the order of 0.173 mm.

VII. REFERENCES

1. Broadbent BH. A new x-ray technique and its application to orthodontia. The Angle Orthodontist 1931;1(2):45-66.

2. Krogman W, Sassouni V. A Syllabus in roentgenographic cephalometry. Copyright Library of congress: Philadelphia 1957;57-9556.

3. Bookstein FL. The geometry of craniofacial invariants. Am J Orthod 1983;83:221-34.

4. Moyers RE, Bookstien FL. The inappropriateness of conventional cephalometrics. Am J Orthod 1979;75(6):599-617.

5. Hixon EH. The norm concept in cephalometrics. Am J Orthod 1956;42:898-906.

6. Melsen B, Baumrind S: Clinical Research Applications of Cephalometry. In: Athanasiou AE, ed. Orthodontic Cephalometry. London: Mosby-Wolfe, 1997.

7. Athanasios AE: Orthodontic cephalometry. London: Mosby-Wolfe, 1997.

8. Macri V, Athanasiou AE: Sources of Error in Lateral Cephalometry. In: Athanasiou AE, ed. Orthodontic Cephalometry. London: Mosby-Wolfe, 1997.

9. Baumrind S, Frantz RC. The reliability of head film measurements. 1. Landmark identification. Am J Orthod 1971;60(2):111-27.

10. Bjork A. The face in profile. Sven Tandlak Tidskr 1947;40((suppl 5B)):1-29.

11. Carlsson GE. Error in X-ray Cephalometry. Odontol Tidskr 1967;75:99-123.

12. Han UK, Vig KWL, Weintraub JA, Vig PS, Kowalski CJ. Consistency of orthodontic treatment decisions relative to diagnostic records. Am J Orthod Dentofac Orthop 1991;100:212-219.

13. Baumrind S: Prediction in the planning and conduct of orthodontic treatment. In: Melsen B, ed. Current Controversies in Orthodontics. Chicago: Quintessence, 1991; 25-44.

14. Bookstein FL: The Inappropriateness of scientific methods in orthodontics. In: Hunter WS, Carlson DS, eds. Craniofacial Growth Series 24. Ann Arbor: Center for Human Growth and Development, 1991.

15. Vig PS: Orthodontic controversies: Their origins, consequences, and resolution. In: Melsen B, ed. Current Controverisies in Orthodontics. Chicago: Quintessence Publishing, 1991; 269-310.

16. Baumrind S, Miller D, Molthen R. The reliability of head film measurements. 3. Tracing superimposition. Am J Orthod 1976;70(6):617-44.

17. Baumrind S, Ben-Bassat Y, Korn EL, Bravo LA, Curry S. Mandibular remodeling measured on cephalograms. 1. Osseous changes relative to superimposition on metallic implants. Am J Orthod Dentofacial Orthop 1992;102(2):134-42.

18. Baumrind S, Ben-Bassat Y, Korn EL, Bravo LA, Curry S. Mandibular remodeling measured on cephalograms: 2. A comparison of information from implant and anatomic best-fit superimpositions. Am J Orthod Dentofacial Orthop 1992;102(3):227-38.

19. Baumrind S, Korn EL, Ben-Bassat Y, West EE. Quantitation of maxillary remodeling. 1. A description of osseous changes relative to superimposition on metallic implants. Am J Orthod Dentofacial Orthop 1987;91(1):29-41.

20. Baumrind S, Korn EL, Ben-Bassat Y, West EE. Quantitation of maxillary remodeling. 2. Masking of remodeling effects when an "anatomical" method of superimposition is used in the absence of metallic implants. Am J Orthod Dentofacial Orthop 1987;91(6):463-74.

21. Gron PA. A geometric evaluation of image size in dental radiography. J Dent Res 1960;39:289-301.

22. Hatcher DC: Maxillofacial Imaging. In: McNeill C, ed. Science and Practice of Occlusion. Chicago: Quintessence Publishing, 1997; 349-364.

23. Broadbent BH, Broadbent BH, Golden W: Bolton standards of dentofacial developmental growth. St. Louis: The CV Mosby Company, 1975.

24. Baumrind S, Moffitt FH, Curry S. Three-dimensional x-ray stereometry from paired coplanar images: A progress report. Am J Orthod 1983;84:292-312.

25. Bookstein FL. On the cephalometrics of skeletal change. Am J Orthod 1982;82(3):177-198.

26. Cutting C, Bookstein FL, Grayson B, Fellingham L, JA M. Three dimensional computer aided design of craniofacial surgical procedures; optimization and interaction with cephalometric CT-based models. Plast Reconst Surg 1986;77:886-7.

27. Cutting C, Grayson B, Bookstein FL, McCarthy JA. Computer aided planning and evaluation of facial and orthognathic surgery. Clin Plast Surg 1986;13:449-62.

28. Baumrind S, Korn EL, Isaacson RJ, West EE, Molthen R. Superimpositional assessment of treatment-associated changes in the temporomandibular joint and the mandibular symphysis. Am J Orthod 1983;84(6):443-65.

29. Bookstein F, Chernoff B, Elder R, Humpheries J, Smith G, Strauss R: Morphometrics in Evolution Biology, Vol. Special Publication No. 15. Philadelphia: Academy of Natural Science, 1985.

30. Quintero JC, Hatcher D, Nielsen IL, Mostafavi H: Three-dimensional cranioacial imaging of condylar position compared to articulator-based condylar position indicator (CPI). . San Francisco: University of California, San Francisco, 1996.

31. Moffitt FH, Mikhail EM: Photogrammetry, 3rd ed. New York: Harper & Row, 1980.

32. Baumrind S, Moffitt FH, Curry S. The geometry of three-dimensional measurements from paired coplanar x-ray images. Am J Orthod 1983;84:313-322.

33. Rune B, Jacobsen S, Sarnas KV, Selvik G. Roentgen stereophotogrammetry applied to the cleft maxilla of infants. I. Implant technique. Scand J Plast Reconstr Surg 1977;11:131.

34. Rune B, Jacobsen S, Sarnas KV, Selvik G. Posterioranterior traction in maxillonasal dysplacia (Binder;s syndrome): A roentgen stereometric study with the aid of metalic implants. Am J Orthod 1982;81:65-70.

35. Karara HM: Non-Topographic Photogrammetry, Second ed: American Society for Photogrammetry and remote Sensing, 1989. (Karara HM, ed.

36. Brown DC: Emerging Trends in Non-Topographic Photogrammetry. In: Karera HM, ed. Non-Topographic Photogrammetry: American Society for Photogrammetry and Remote Sensing, 1989; 367.

37. Landis JR, Koch GG. A Review of Statistical methods in the Analysis of Data Arising From Observer Reliability Studies (Part I). Statistica Neerlandica 1975;29(3):101-123.

38. Glantz SA: Primer of Bio-statistics, Fourth ed. New York: McGraw-Hill, 1997.

Figure 6. Box Physical Measurements
Mean vs. Variance

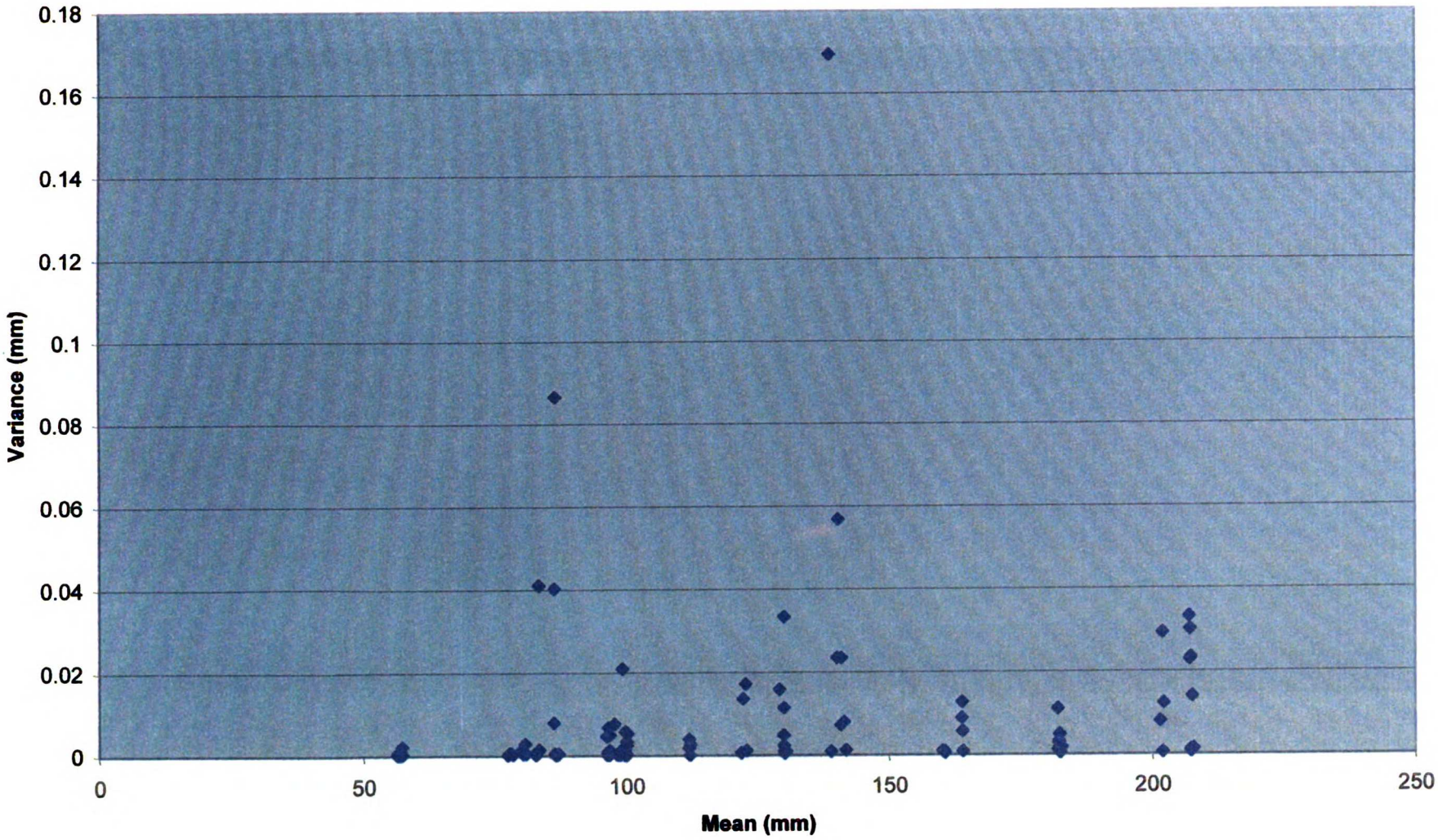

Figure 7. Skull Physical Measurements
Mean vs. Variance

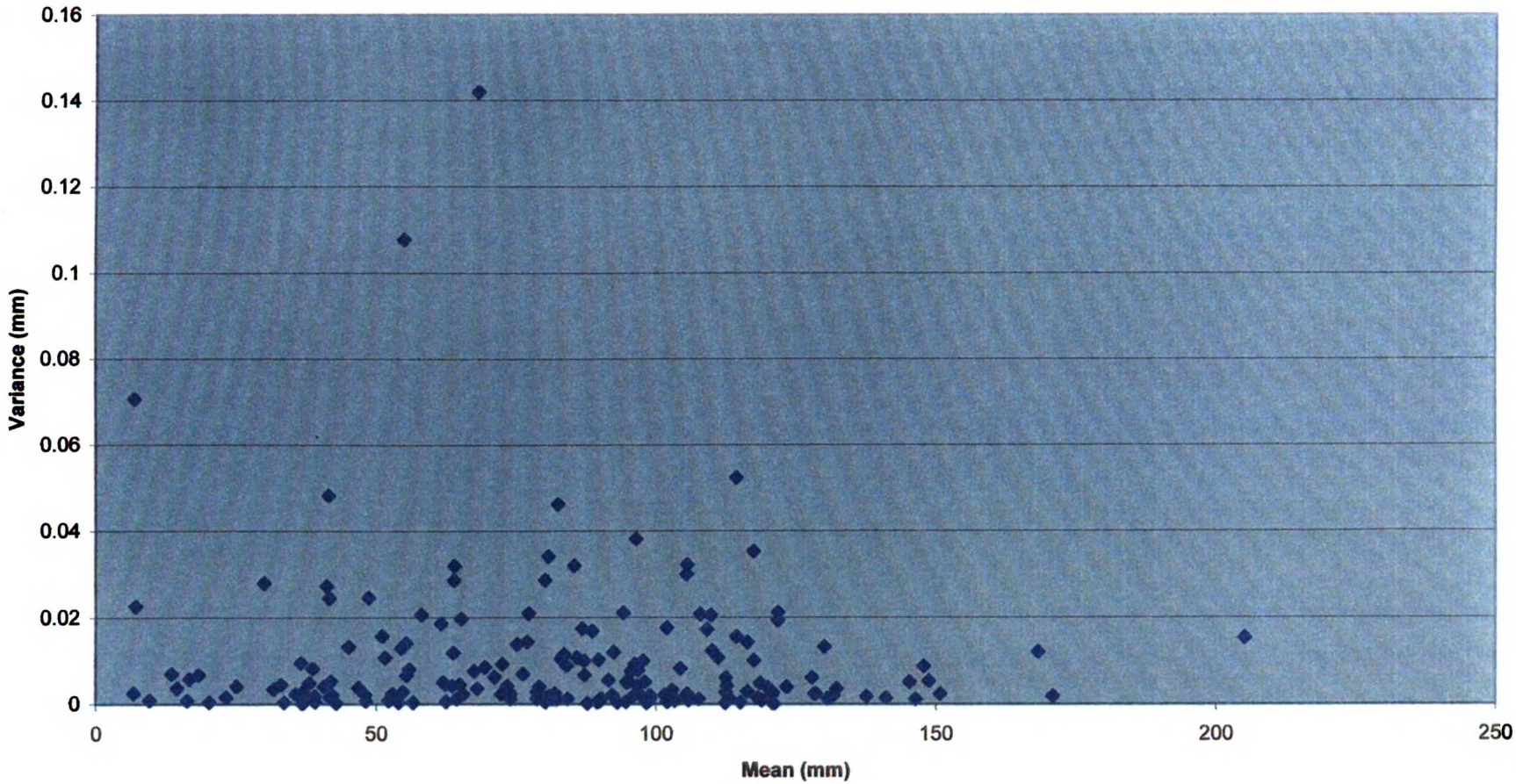

Figure 8. Skull Radiographic Measurements
Mean vs. Variance

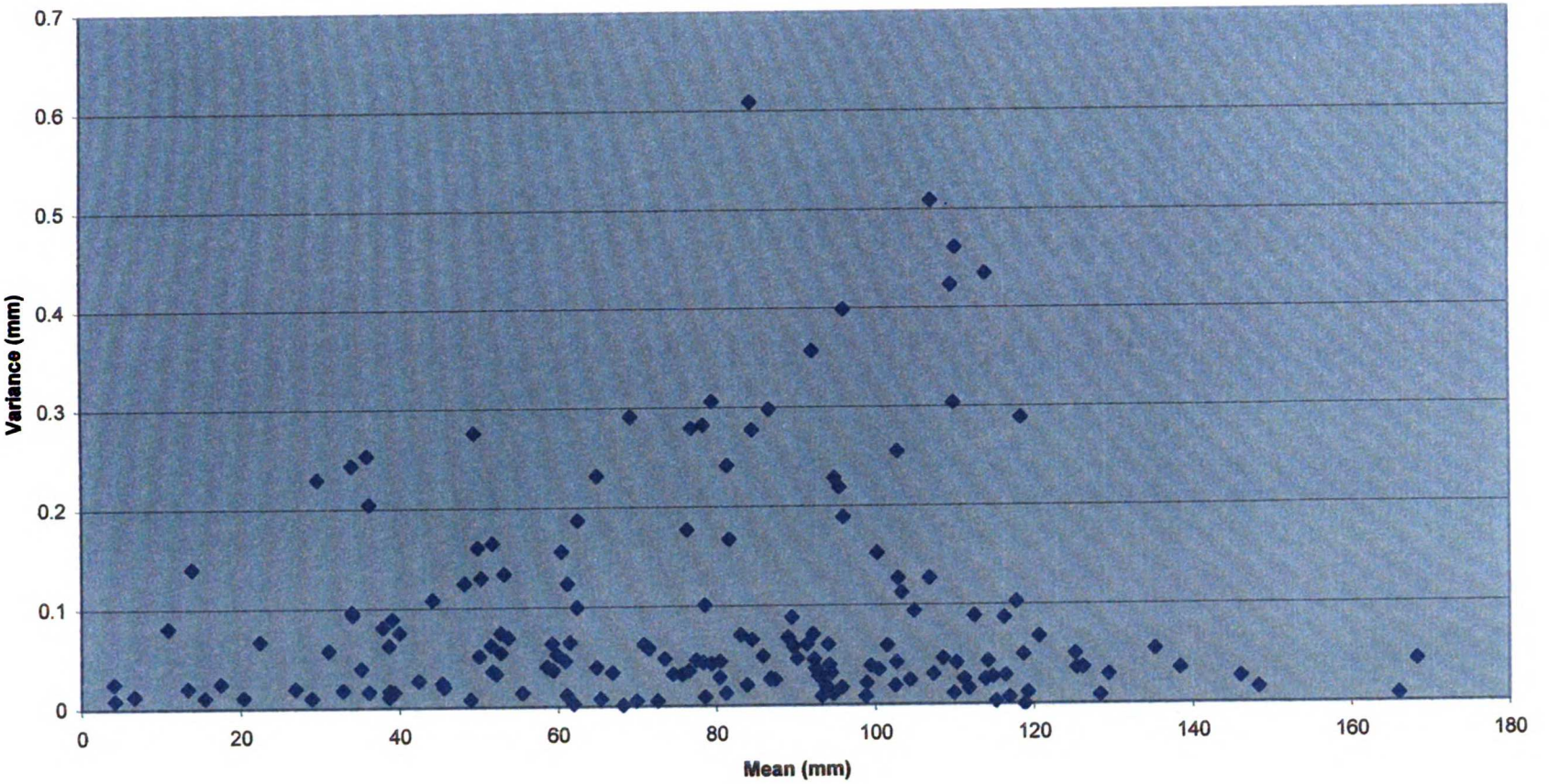

Figure 9. Skull Photographic Measurements
Mean vs. Variance

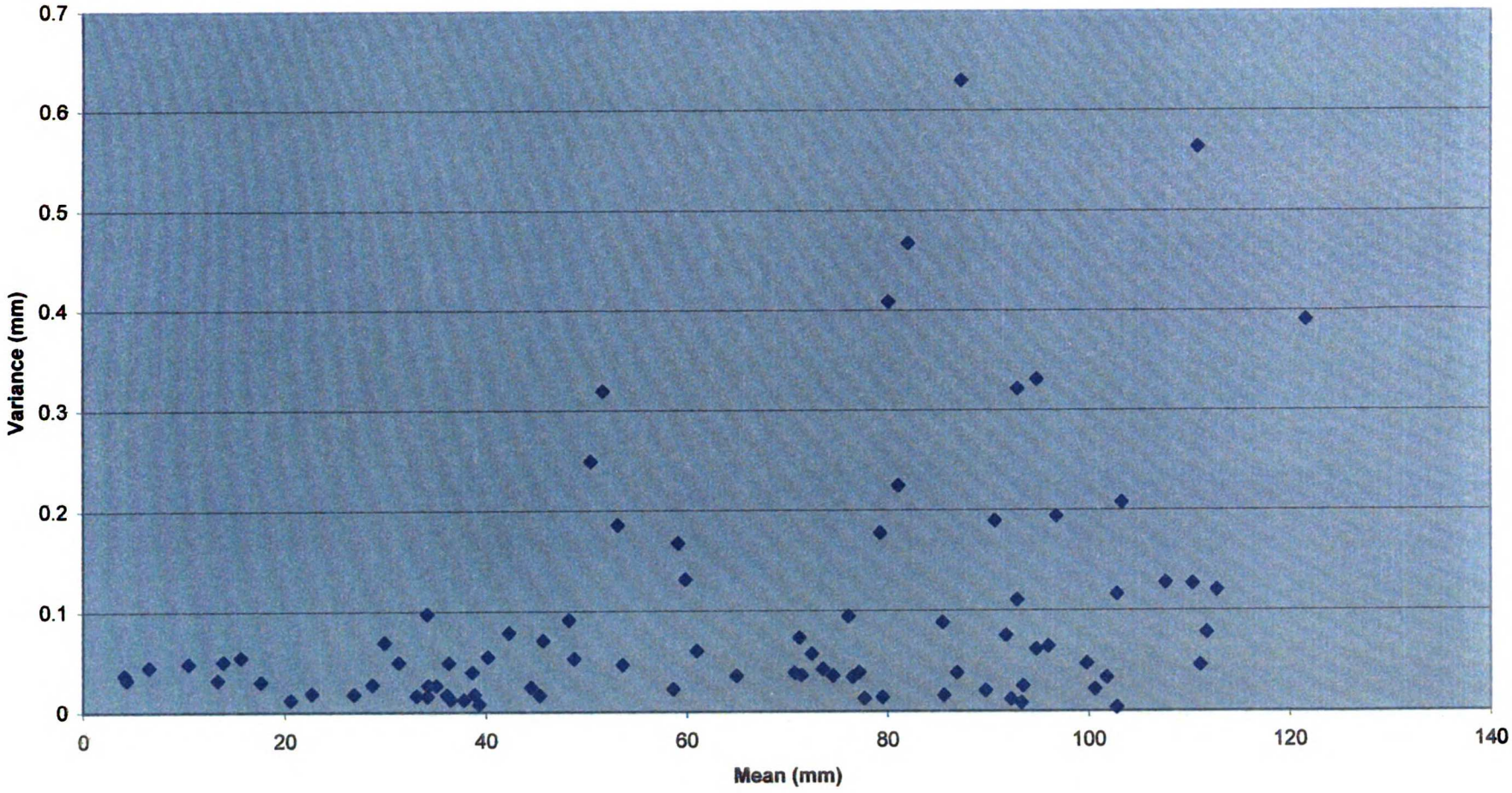

Figure 10. Correlation Between Skull Radiographic and Physical Measurements

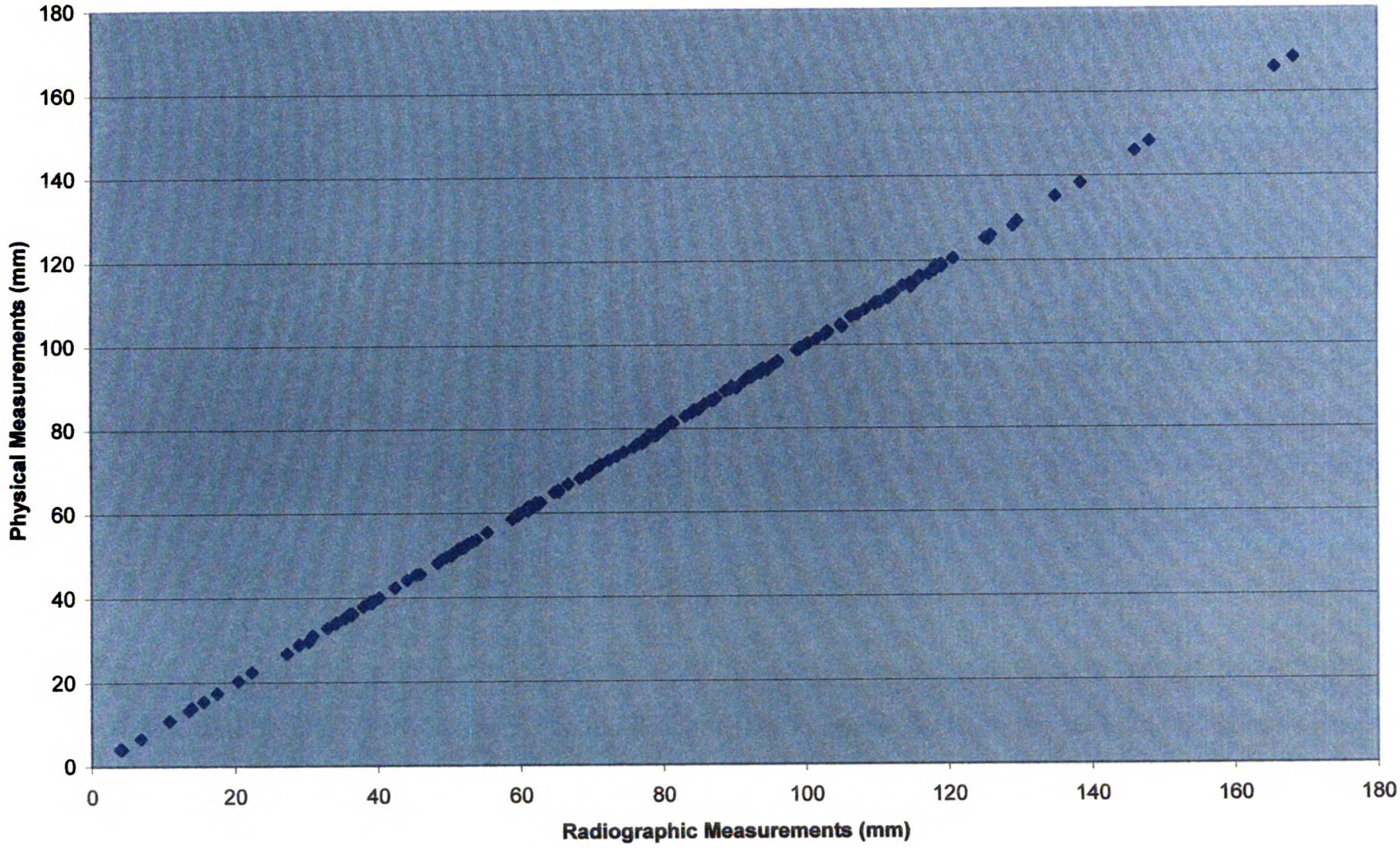

Figure 11. Correlation Between Skull Photographic and Physical Measurements

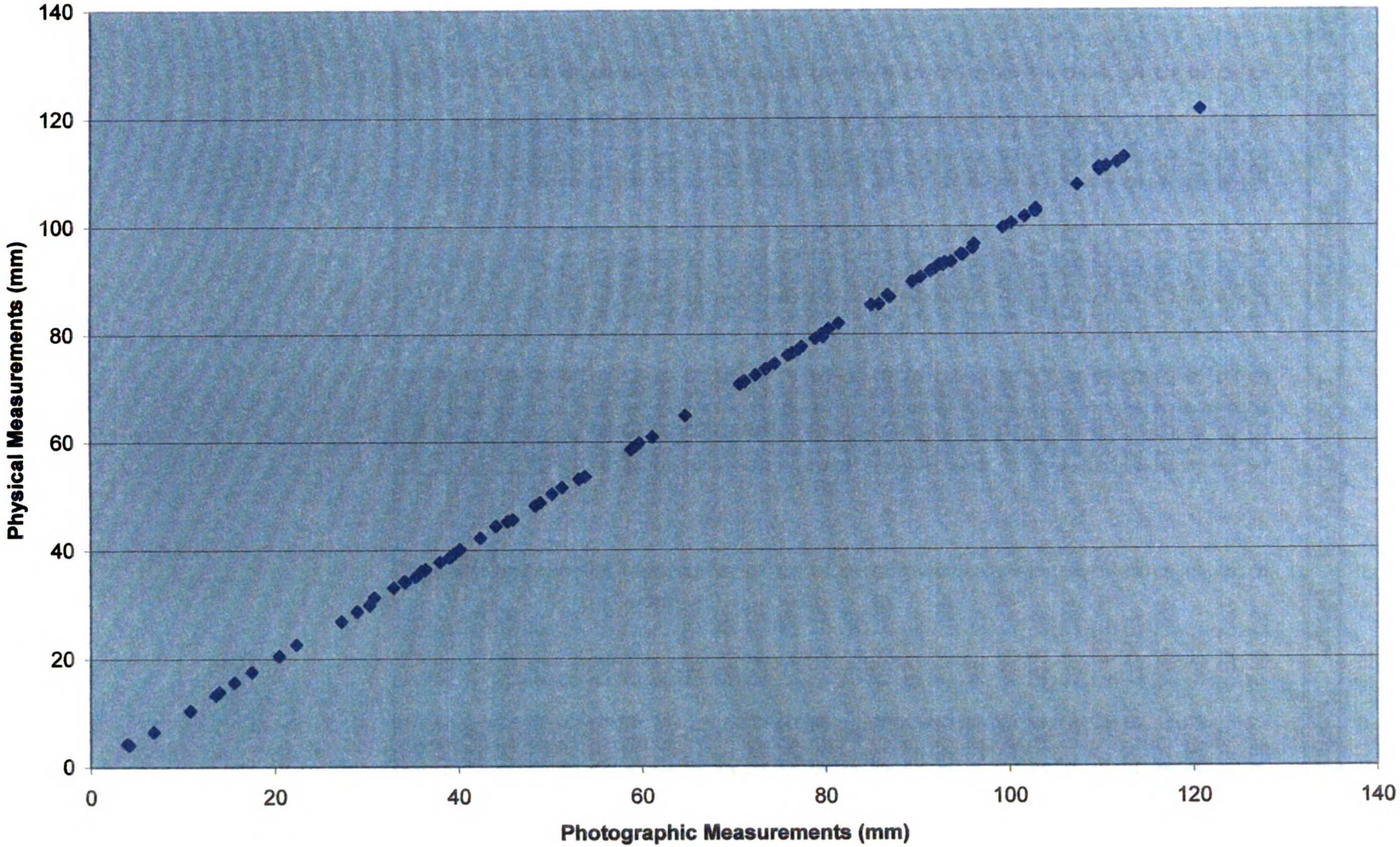

Table 2. Gold Standard Physical Linear Measurements (mm) for Boxes A and B

LOCATION	N	Mean	Variance	*LOCATION*	N	Mean	Variance
A12-A23	5	99.866	0.00593	B12-B23	5	87.112	0.00055
A12-A34	5	140.336	0.05693	B12-B34	5	122.732	0.0173
A12-A41	5	99.03	0.00037	B12-B41	5	86.65	0.00017
A12-A'12	5	182.254	0.00337	B12-B'12	5	160.584	0.00087
A12-A'23	5	207.8	0.00142	B12-B'23	5	182.77	0.00187
A12-A'41	5	207.532	0.0141	B12-B'34	5	201.9	0.02947
A23-A34	5	99.002	0.00125	B12-B'41	5	182.414	0.00127
A23-A41	5	140.102	0.0236	B23-B34	5	86.836	0.00028
A23-A'12	5	207.328	0.00073	B23-B41	5	122.894	0.00122
A23-A'23	5	182.494	0.00047	B23-B'12	5	182.34	0.00492
A23-A'34	5	207.338	0.00123	B23-B'23	5	160.612	0.00055
A34-A41	5	98.906	0.00023	B23-B'34	5	182.26	0.00287
A34-A'23	5	206.954	0.03327	B23-B'41	5	201.924	0.00057
A34-A'34	5	182.034	0.01117	B34-B41	5	86.742	0.0004
A34-A'41	5	207.294	0.02352	B34-B'12	5	201.488	0.00808
A41-A'12	5	207.106	0.03023	B34-B'23	5	182.296	0.00298
A41-A'34	5	207.094	0.02297	B34-B'34	5	160.158	0.00098
A41-A'41	5	182.296	0.00173	B34-B'41	5	182.112	0.0012
A'12-A'23	5	98.212	0.00035	B41-B'12	5	182.382	0.0006
A'12-A'34	5	139	0.00097	B41-B'23	5	202.156	0.01243
A'12-A'41	5	98.536	0.00033	B41-B'34	5	182.486	0.00493
A'23-A'34	5	97.776	0.00778	B41-B'41	5	160.508	0.00083
A'23-A'41	5	138.718	0.16958	B'12-B'23	5	86.576	0.08673
A'34-A'41	5	98.448	0.00028	B'12-B'34	5	121.91	0.00067
				B'12-B'41	5	86.284	0.04037
				B'23-B'34	5	86.242	0.0081
				B'23-B'41	5	122.26	0.01377
				B'34-B'41	5	86.418	0.00053

Table 3. Gold Standard Physical Linear Measurements (mm) for Boxes C and D

LOCATION	N	Mean	Variance	*LOCATION*	N	Mean	Variance
C12-C23	5	100.168	0.00028	D12-D23	5	57.446	0.00038
C12-C34	5	141.826	0.00128	D12-D34	5	80.774	0.00297
C12-C41	5	100.292	0.00545	D12-D41	5	57.366	0.00228
C12-C'12	5	83.358	0.04113	D12-D'12	5	77.902	0.00065
C12-C'23	5	130.466	0.00103	D12-D'23	5	96.81	0.00137
C12-C'34	5	163.828	0.00898	D12-D'34	5	112.256	0.00273
C12-C'41	5	130.062	0.03345	D12-D'41	5	96.298	0.00478
C23-C34	5	100.058	0.00348	D23-D34	5	56.728	0.00053
C23-C41	5	141.454	0.00817	D23-D41	5	80.91	0.00052
C23-C'12	5	129.998	0.00243	D23-D'12	5	96.508	0.00013
C23-C'23	5	83.428	0.00153	D23-D'23	5	78.194	0.00057
C23-C'34	5	130.034	0.00097	D23-D'34	5	96.57	0.00042
C23-C'41	5	163.882	0.01285	D23-D'41	5	111.972	0.00405
C34-C41	5	100.142	0.00255	D34-D41	5	57	0.00107
C34-C'12	5	164.034	0.00092	D34-D'12	5	111.96	0.00187
C34-C'23	5	129.976	0.00493	D34-D'23	5	96.854	0.00507
C34-C'34	5	82.81	0.00022	D34-D'34	5	78.442	0.0003
C34-C'41	5	130.198	0.00053	D34-D'41	5	96.714	0.00012
C41-C'12	5	130.008	0.01158	D41-D'12	5	96.438	0.00073
C41-C'23	5	163.958	0.00578	D41-D'23	5	112.156	0.00018
C41-C'34	5	129.18	0.01597	D41-D'34	5	96.588	0.00688
C41-C'41	5	82.996	0.00103	D41-D'41	5	77.494	0.00022
C'12-C'23	5	99.806	0.00013	D'12-D'23	5	56.46	0.00027
C'12-C'34	5	140.81	0.00737	D'12-D'34	5	79.976	0.00123
C'12-C'41	5	99.706	0.00153	D'12-D'41	5	56.586	0.00073
C'23-C'34	5	99.874	0.00047	D'23-D'34	5	56.732	0.00015
C'23-C'41	5	140.964	0.02357	D'23-D'41	5	80.424	0.00047
C'34-C'41	5	99.316	0.02108	D'34-D'41	5	57.116	0.00033

Table 4. Gold Standard Physical Linear Measurements (mm)
Skull A

LOCATION	N	Mean (mm)	Variance	LOCATION	N	Mean (mm)	Variance
Bgma-CmaL	5	75.946	0.00123	CmaR-Gn	5	168.202	0.00185
Bgma-CmaR	5	74.192	0.01445	G-ZygL	5	87.438	0.00133
Bgma-G	5	100.596	0.00083	G-ZygR	5	84.078	0.01743
Bgma-ZygL	5	127.914	0.00142	G-MasL	5	129.568	0.00363
Bgma-ZygR	5	127.38	0.01332	G-MasR	5	129.002	0.00205
Bgma-MasL	5	143.66	0.00122	G-ANS	5	55.296	0.02063
Bgma-MasR	5	142.556	0.00518	G-Gn	5	125.148	0.00623
Bgma-ANS	5	145.124	0.00882	ZygL-ZygR	5	120.648	0.00403
Bgma-Gn	5	202.338	0.01533	ZygL-MasL	5	59.652	0.0046
CmaL-CmaR	5	118.18	0.00272	ZygL-MasR	5	125.554	0.00247
CmaL-G	5	84.482	0.00675	ZygL-ANS	5	80.364	0.01077
CmaL-ZygL	5	65.3	0.00367	ZygL-Gn	5	109.734	0.00277
CmaL-ZygR	5	134.902	0.0018	ZygR-MasL	5	125.88	0.00247
CmaL-MasL	5	98.786	0.00213	ZygR-MasR	5	62.45	0.01972
CmaL-MasR	5	146.024	0.00542	ZygR-ANS	5	75.938	0.00288
CmaL-ANS	5	114.692	0.03525	ZygR-Gn	5	107.322	0.0124
CmaL-Gn	5	165.556	0.01213	MasL-MasR	5	100.406	0.00148
CmaR-G	5	87.166	0.00073	MasL-ANS	5	115.418	0.00148
CmaR-ZygL	5	138.394	0.00142	MasL-Gn	5	119.028	0.02113
CmaR-ZygR	5	68.392	0.00635	MasR-ANS	5	114.762	0.0102
CmaR-MasL	5	148.044	0.00242	MasR-Gn	5	119.058	0.01933
CmaR-MasR	5	99.132	0.01765	ANS-Gn	5	70.688	0.00428
CmaR-ANS	5	117.278	0.00388				

Table 5. Gold Standard Physical Linear Measurements (mm)
Skull B

LOCATION	N	Mean (mm)	Variance	LOCATION	N	Mean (mm)	Variance	LOCATION	N	Mean (mm)	Variance
Pclin-N	5	60.99	0.01187	OrbL-CoL	5	69.574	0.00232	ANS-GoR	5	94.702	0.00185
Pclin-OrbL	5	61.618	0.00118	OrbL-PoL	5	84.358	0.01003	ANS-PNS	5	52.014	0.00287
Pclin-OrbR	5	62.758	0.00228	OrbL-PoR	5	111.58	0.05237	A-CoL	5	95.246	0.00523
Pclin-ANS	5	77.458	0.00048	OrbL-B	5	72.406	0.01388	A-PoL	5	109.754	0.00617
Pclin-A	5	79.162	0.00255	OrbL-Gn	5	92.936	0.00158	A-B	5	42.354	0.01332
Pclin-Col	5	61.122	0.0286	OrbL-GoL	5	86.77	0.00047	A-Gn	5	64.724	0.00767
Pclin-B	5	103.078	0.00098	OrbL-GoR	5	110.428	0.00133	A-GoL	5	92.386	0.00528
Pclin-GoL	5	88.788	0.00563	OrbL-PNS	5	50.424	0.00172	A-GoR	5	90.338	0.00043
Pclin-GoR	5	92.046	0.00508	OrbR-ANS	5	35.308	0.00493	A-PNS	5	50.298	0.00143
N-OrbL	5	38.716	0.04828	OrbR-A	5	37.934	0.00412	CoL-PoR	5	108.342	0.01085
N-OrbR	5	38.88	0.02447	OrbR-Col	5	103.102	0.0016	CoL-B	5	104.938	0.00123
N-A	5	52.584	0.01412	OrbR-PoL	5	113.596	0.00293	CoL-Gn	5	116.192	0.00095
N-CoL	5	96.122	0.0021	OrbR-B	5	71.222	0.0024	CoL-GoL	5	51.758	0.01298
N-PoL	5	107.046	0.02053	OrbR-Gn	5	91.922	0.00055	CoL-GoR	5	113.586	0.01433
N-PoR	5	105.136	0.02073	OrbR-GoL	5	109.68	0.00032	CoL-PNS	5	62.134	0.00452
N-B	5	93.854	0.00432	OrbR-GoR	5	84.996	0.00023	PoL-PoR	5	106.356	0.01723
N-Gn	5	115.894	0.00492	OrbR-PNS	5	49.468	0.00083	B-Gn	5	22.328	0.00413
N-GoL	5	118.338	3.00E-05	ANS-A	5	6.842	0.00085	B-GoL	5	79.638	0.00123
N-GoR	5	118.034	0.00237	ANS-CoL	5	95.608	0.00033	B-GoR	5	77.088	0.00173
N-PNS	5	65.328	0.14193	ANS-PoL	5	109.97	0.00432	Gn-GoL	5	81.462	0.00125
OrbL-OrbR	5	53.122	0.00815	ANS-B	5	48.86	0.01082	Gn-GoR	5	78.918	0.00128
OrbL-ANS	5	35.932	0.00825	ANS-Gn	5	71.186	0.00118	Gn-PNS	5	78.324	0.00127
OrbL-A	5	39.442	0.00215	ANS-GoL	5	96.134	0.00127	GoL-GoR	5	89.68	0.01207

Table 6. Gold Standard Physical Linear Measurements (mm)
Skull C

LOCATION	N	Mean (mm)	Variance	LOCATION	N	Mean (mm)	Variance	LOCATION	N	Mean (mm)	Variance
N-FzL	5	52.656	0.00673	FzL-LR6A	5	112.376	0.00043	UL1I-LL1I	5	4.188	0.07073
N-FzR	5	52.196	0.10783	FzL-LR6MB	5	102.5	0.00157	UL1I-UL6MB	5	34.172	0.00095
N-UL1A	5	60.79	0.00427	FzR-UL1A	5	79.742	0.04625	UL1I-UR6MB	5	39.146	0.00533
N-UL1I	5	78.08	0.00187	FzR-UL1I	5	93.65	0.03817	LL1A-LL1I	5	13.548	0.00083
N-LL1A	5	92.094	0.00527	FzR-LL1A	5	102.72	0.02997	LL1A-UL6A	5	44.054	0.00382
N-LL1I	5	80.826	0.01153	FzR-LL1I	5	94.93	0.01012	LL1A-LL6A	5	30.818	0.00038
N-UL6A	5	66.656	0.00863	FzR-UL6A	5	92.8	0.00767	LL1A-UR6A	5	45.89	0.02457
N-UL6MB	5	80.292	0.01045	FzR-UL6MB	5	101.618	0.00833	LL1A-LR6A	5	34.168	0.00283
N-LL6A	5	93.5	0.00932	FzR-LL6A	5	111.642	0.0156	LL1I-LL6MB	5	30.284	0.00452
N-LL6MB	5	83.122	0.0108	FzR-LL6MB	5	102.84	0.03217	LL1I-LR6MB	5	33.822	0.00955
N-UR6A	5	69.752	0.00935	FzR-UR6A	5	61.166	0.03193	UL6A-UL6MB	5	15.6	0.00677
N-UR6MB	5	81.228	0.00893	FzR-UR6MB	5	74.496	0.02088	UL6A-LL6A	5	28.944	0.00347
N-LR6A	5	94.03	0.00787	FzR-LR6A	5	86.992	0.0103	UL6A-UR6A	5	53.79	0.00037
N-LR6MB	5	82.61	0.03197	FzR-LR6MB	5	78.022	0.0341	UL6A-LR6A	5	59.698	0.00058
FzL-FzR	5	99.262	0.00055	UL1A-UL1I	5	17.482	0.00045	UL6MB-LL6MB	5	3.966	0.00253
FzL-UL1A	5	76.406	0.00403	UL1A-LL1A	5	32.9	0.00237	UL6MB-UR6MB	5	50.184	0.00242
FzL-UL1I	5	89.436	0.00218	UL1A-LL1I	5	20.462	0.0016	LL6A-LL6MB	5	10.818	0.00703
FzL-LL1A	5	100.172	0.00335	UL1A-UL6A	5	34.068	8.00E-05	LL6A-UR6A	5	59.192	0.00505
FzL-LL1I	5	91.412	0.02105	UL1A-UL6MB	5	36.368	0.00048	LL6A-LR6A	5	51.262	0.0004
FzL-UL6A	5	58.816	0.01863	UL1A-LL6A	5	45.312	0.00215	LL6MB-LR6MB	5	45.376	0.00073
FzL-UL6MB	5	73.504	0.00702	UL1A-LL6MB	5	36.286	0.00178	UR6A-UR6MB	5	13.958	0.00583
FzL-LL6A	5	85.85	0.01687	UL1A-UR6A	5	38.95	0.00157	UR6A-LR6A	5	27.236	0.02793
FzL-LL6MB	5	77.434	0.02867	UL1A-UR6MB	5	40.126	0.00023	UR6MB-LR6MB	5	4.35	0.02257
FzL-UR6A	5	95.976	0.00073	UL1A-LR6A	5	48.34	0.01577	LR6A-LR6MB	5	11.748	0.00373
FzL-UR6MB	5	102.816	0.00243	UL1A-LR6MB	5	38.386	0.02723				

Table 7. Digital Radiographic 3-D Linear Measurements (mm)
Skull A

LOCATION	N	Mean (mm)	Variance	LOCATION	N	Mean (mm)	Variance
Bgma-CmaL	0			CmaR-Gn	5	168.2685038	0.042373569
Bgma-CmaR	0			G-ZygL	5	87.34708964	0.026216642
Bgma-G	0			G-ZygR	5	83.83432145	0.020940897
Bgma-ZygL	0			G-MasL	5	129.4126079	0.02950611
Bgma-ZygR	0			G-MasR	5	128.3341435	0.008708092
Bgma-MasL	0			G-ANS	5	55.48605546	0.014473375
Bgma-MasR	0			G-Gn	5	125.3928476	0.036559781
Bgma-ANS	0			ZygL-ZygR	5	120.6595552	0.068395939
Bgma-Gn	0			ZygL-MasL	5	59.33617677	0.037094302
CmaL-CmaR	5	118.880378	0	ZygL-MasR	5	125.1831683	0.050778218
CmaL-G	5	84.4857222	0.06659711	ZygL-ANS	5	80.40258312	0.028820676
CmaL-ZygL	5	65.3574523	0.00767183	ZygL-Gn	5	109.9586466	0.011147694
CmaL-ZygR	5	135.265698	0.0548345	ZygR-MasL	5	126.1741953	0.036698398
CmaL-MasL	5	98.8109655	0.00861862	ZygR-MasR	5	61.95966711	0.002901603
CmaL-MasR	5	146.048234	0.02659953	ZygR-ANS	5	75.6302314	0.031932911
CmaL-ANS	5	114.830156	0.02758687	ZygR-Gn	5	107.356116	0.030452599
CmaL-Gn	5	165.982687	0.00793882	MasL-MasR	5	100.4502415	0.035530709
CmaR-G	5	86.7675344	0.02649053	MasL-ANS	5	115.2279608	0.002900755
CmaR-ZygL	5	138.401288	0.03551603	MasL-Gn	5	119.2433855	0.01201589
CmaR-ZygR	5	68.194276	0.00156119	MasR-ANS	5	113.889916	0.025155139
CmaR-MasL	5	148.315814	0.01529345	MasR-Gn	5	118.6702988	0.050212363
CmaR-MasR	5	98.9346116	0.02209418	ANS-Gn	5	70.81487057	0.062518707
CmaR-ANS	5	116.930676	0.00704376				

Table 8. Digital Radiographic 3-D Linear Measurements (mm)
Skull B

LOCATION	N	Mean (mm)	Variance	LOCATION	N	Mean (mm)	Variance	LOCATION	N	Mean (mm)	Variance
Pclin-N	5	60.4541406	0.15584941	OrbL-CoL	5	69.25262351	0.291561	ANS-GoR	5	94.0861608	0.06145499
Pclin-OrbL	5	61.2004549	0.12401458	OrbL-PoL	5	84.49735876	0.609117	ANS-PNS	5	51.7630333	0.16472783
Pclin-OrbR	5	62.5069755	0.18723026	OrbL-PoR	5	111.2058768	0.025698	A-CoL	5	94.9171968	0.22864111
Pclin-ANS	5	76.9143191	0.27951103	OrbL-B	5	72.54996081	0.00542	A-PoL	5	109.778656	0.42367588
Pclin-A	5	78.4149279	0.28272028	OrbL-Gn	5	93.20685419	0.030208	A-B	5	42.4017077	0.02721188
Pclin-Col	5	61.4708808	0.06506499	OrbL-GoL	5	86.75546173	0.298354	A-Gn	5	64.8473548	0.03973054
Pclin-B	5	102.917086	0.12692381	OrbL-GoR	5	110.2722488	0.041966	A-GoL	5	92.2349658	0.35758872
Pclin-GoL	5	89.0406045	0.06843587	OrbL-PNS	5	50.31512297	0.130153	A-GoR	5	89.7172987	0.05948573
Pclin-GoR	5	92.2871155	0.04642976	OrbR-ANS	5	35.18351201	0.039894	A-PNS	5	49.912683	0.1603878
N-OrbL	5	38.7151017	0.01089084	OrbR-A	5	37.88429955	0.081497	CoL-PoR	5	108.550887	0.04633791
N-OrbR	5	39.0883671	0.08963803	OrbR-Col	5	103.3611404	0.112731	CoL-B	5	104.930339	0.09432154
N-A	5	52.7589335	0.05511959	OrbR-PoL	5	114.1223554	0.435419	CoL-Gn	5	116.278998	0.08711843
N-CoL	5	96.0255676	0.18884684	OrbR-B	5	71.44400484	0.058478	CoL-GoL	5	51.7601647	0.03631285
N-PoL	5	107.271749	0.50963976	OrbR-Gn	5	92.18646546	0.071823	CoL-GoR	5	114.204925	0.04345257
N-PoR	5	104.3805	0.02495257	OrbR-GoL	5	110.0234066	0.304199	CoL-PNS	5	62.3595226	0.10008046
N-B	5	94.2211792	0.04083472	OrbR-GoR	5	84.59380657	0.277731	PoL-PoR	5	106.863299	0.12685016
N-Gn	5	116.437344	0.02916231	OrbR-PNS	5	49.49327246	0.276043	B-Gn	5	22.4468381	0.06785699
N-GoL	5	118.496801	0.28881467	ANS-A	5	6.619665191	0.013116	B-GoL	5	79.5589149	0.3066714
N-GoR	5	117.777285	0.10288573	ANS-CoL	5	95.53133557	0.21926	B-GoR	5	76.5007102	0.03545593
N-PNS	5	64.9617211	0.23224698	ANS-PoL	5	110.3225723	0.461796	Gn-GoL	5	81.4137691	0.24177678
OrbL-OrbR	5	53.2053257	0.13395345	ANS-B	5	48.95489322	0.007826	Gn-GoR	5	78.324199	0.04387848
OrbL-ANS	5	36.1345264	0.01641946	ANS-Gn	5	71.39869643	0.058747	Gn-PNS	5	78.540251	0.10146382
OrbL-A	5	39.3071989	0.01582355	ANS-GoL	5	96.21432764	0.399387	GoL-GoR	5	90.1635534	0.04751123

Table 9. Digital Radiographic 3-D Linear Measurements (mm)
Skull C

LOCATION	N	Mean (mm)	Variance	LOCATION	N	Mean (mm)	Variance	LOCATION	N	Mean (mm)	Variance
N-FzL	5	52.764049	0.074936	FzL-LR6A	5	112.496536	0.089028	UL1I-LL1I	5	4.06159209	0.02566641
N-FzR	5	52.1946348	0.033794	FzL-LR6MB	0			UL1I-UL6MB	5	34.0300729	0.24402208
N-UL1A	5	61.0742677	0.011875	FzR-UL1A	5	79.3756936	0.042357	UL1I-UR6MB	5	38.7733306	0.01705817
N-UL1I	5	78.5427058	0.009109	FzR-UL1I	5	93.2877319	0.009299	LL1A-LL1I	5	13.3591741	0.02074598
N-LL1A	5	92.4792743	0.036909	FzR-LL1A	5	102.529211	0.019281	LL1A-UL6A	5	44.1662444	0.10861656
N-LL1I	5	81.1817009	0.012857	FzR-LL1I	5	94.6627997	0.011397	LL1A-LL6A	5	31.0811693	0.0582947
N-UL6A	5	66.8345769	0.034312	FzR-UL6A	5	92.8697466	0.029344	LL1A-UR6A	5	45.6081327	0.02055177
N-UL6MB	5	80.463792	0.044939	FzR-UL6MB	5	101.517127	0.05983	LL1A-LR6A	5	34.1130456	0.09430292
N-LL6A	5	93.7906918	0.01966	FzR-LL6A	5	111.82702	0.016031	LL1I-LL6MB	5	29.6993987	0.2302554
N-LL6MB	5	83.0468674	0.071538	FzR-LL6MB	5	102.692907	0.04275	LL1I-LR6MB	0		
N-UR6A	5	69.9099665	0.005674	FzR-UR6A	5	60.8953985	0.046526	UL6A-UL6MB	5	15.5037723	0.01116559
N-UR6MB	5	81.6351509	0.167113	FzR-UR6MB	5	74.5096946	0.032213	UL6A-LL6A	5	28.938342	0.01046371
N-LR6A	5	94.4343352	0.032345	FzR-LR6A	5	86.8452267	0.027422	UL6A-UR6A	5	53.6857006	0.07029367
N-LR6MB	0			FzR-LR6MB	0			UL6A-LR6A	5	59.8184007	0.05320958
FzL-FzR	5	99.4590046	0.039578	UL1A-UL1I	5	17.4848676	0.025256	UL6MB-LL6MB	5	4.1860556	0.00882616
FzL-UL1A	5	76.3093293	0.177067	UL1A-LL1A	5	32.8744622	0.018009	UL6MB-UR6MB	5	50.0616417	0.0519561
FzL-UL1I	5	89.4975812	0.088533	UL1A-LL1I	5	20.3821741	0.011358	LL6A-LL6MB	5	10.8889301	0.08146328
FzL-LL1A	5	100.281431	0.152138	UL1A-UL6A	5	34.0158212	0.096955	LL6A-UR6A	5	59.2481805	0.06417891
FzL-LL1I	5	91.4094577	0.061462	UL1A-UL6MB	5	36.2406987	0.204885	LL6A-LR6A	5	51.5326074	0.06263517
FzL-UL6A	5	58.5861566	0.040666	UL1A-LL6A	5	45.3825965	0.024607	LL6MB-LR6MB	0		
FzL-UL6MB	5	73.4439554	0.047915	UL1A-LL6MB	5	35.967403	0.253762	UR6A-UR6MB	5	13.8927994	0.14056454
FzL-LL6A	5	85.8534446	0.049983	UL1A-UR6A	5	38.6901271	0.062964	UR6A-LR6A	5	26.8810685	0.02019597
FzL-LL6MB	5	77.4229444	0.046236	UL1A-UR6MB	5	39.9918114	0.076002	UR6MB-LR6MB	0		
FzL-UR6A	5	95.7969803	0.017799	UL1A-LR6A	5	48.211485	0.12481	LR6A-LR6MB	0		
FzL-UR6MB	5	102.9228	0.255219	UL1A-LR6MB	0						

Table 10. Digital Photographic 3-D Linear Measurements (mm)
Skull A

LOCATION	N	Mean (mm)	Variance	LOCATION	N	Mean	Variance
Bgma-CrnaL	0			CrnaR-Gn	0		
Bgma-CrnaR	0			G-ZygL	0		
Bgma-G	0			G-ZygR	0		
Bgma-ZygL	0			G-MasL	0		
Bgma-ZygR	0			G-MasR	0		
Bgma-MasL	0			G-ANS	0		
Bgma-MasR	0			G-Gn	0		
Bgma-ANS	0			ZygL-ZygR	5	121.625966	0.391121577
Bgma-Gn	0			ZygL-MasL	0		
CrnaL-CrnaR	0			ZygL-MasR	0		
CrnaL-G	0			ZygL-ANS	5	81.0362522	0.22479084
CrnaL-ZygL	0			ZygL-Gn	5	110.300577	0.126745177
CrnaL-ZygR	0			ZygR-MasL	0		
CrnaL-MasL	0			ZygR-MasR	0		
CrnaL-MasR	0			ZygR-ANS	5	76.0845955	0.094763497
CrnaL-ANS	0			ZygR-Gn	5	107.603256	0.127498728
CrnaL-Gn	0			MasL-MasR	0		
CrnaR-G	0			MasL-ANS	0		
CrnaR-ZygL	0			MasL-Gn	0		
CrnaR-ZygR	0			MasR-ANS	0		
CrnaR-MasL	0			MasR-Gn	0		
CrnaR-MasR	0			ANS-Gn	5	70.7571419	0.038867334
CrnaR-ANS	0						

Table 11. Digital Photographic 3-D Linear Measurements (mm)
Skull B

LOCATION	N	Mean (mm)	Variance	LOCATION	N	Mean (mm)	Variance	LOCATION	N	Mean (mm)	Variance
Pclin-N	0			OrbL-CoL	0			ANS-GoR	5	94.8480306	0.331352
Pclin-OrbL	0			OrbL-PoL	0			ANS-PNS	0		
Pclin-OrbR	0			OrbL-PoR	0			A-CoL	0		
Pclin-ANS	0			OrbL-B	5	72.4422049	0.057808	A-PoL	0		
Pclin-A	0			OrbL-Gn	5	93.3156598	0.008266	A-B	5	42.2787165	0.079341
Pclin-Col	0			OrbL-GoL	5	87.2772166	0.630614	A-Gn	5	64.939847	0.03595
Pclin-B	0			OrbL-GoR	5	111.07785	0.045994	A-GoL	5	92.9459352	0.321906
Pclin-GoL	0			OrbL-PNS	0			A-GoR	5	90.6437494	0.189536
Pclin-GoR	0			OrbR-ANS	5	35.0328784	0.026587	A-PNS	0		
N-OrbL	0			OrbR-A	5	37.7998259	0.012346	CoL-PoR	0		
N-OrbR	0			OrbR-Col	0			CoL-B	0		
N-A	0			OrbR-PoL	0			CoL-Gn	0		
N-CoL	0			OrbR-B	5	71.2078902	0.073805	CoL-GoL	0		
N-PoL	0			OrbR-Gn	5	92.2857605	0.011895	CoL-GoR	0		
N-PoR	0			OrbR-GoL	5	110.818226	0.564023	CoL-PNS	0		
N-B	0			OrbR-GoR	5	85.4675899	0.088501	PoL-PoR	0		
N-Gn	0			OrbR-PNS	0			B-Gn	5	22.6698482	0.018902
N-GoL	0			ANS-A		6.53398956	0.04517	B-GoL	5	80.103911	0.409309
N-GoR	0			ANS-CoL	0			B-GoR	5	77.1475002	0.039089
N-PNS	0			ANS-PoL	0			Gn-GoL	5	82.0579597	0.467887
OrbL-OrbR	5	53.09051323	0.185838	ANS-B	5	48.7623477	0.053434	Gn-GoR	5	79.2107451	0.177429
OrbL-ANS	5	36.09823082	0.017324	ANS-Gn	5	71.4154061	0.036414	Gn-PNS	0		
OrbL-A	5	39.32184593	0.008018	ANS-GoL	5	96.7568361	0.194113	GoL-GoR	0		

Table 12. Digital Photographic 3-D Linear Measurements (mm)
Skull C

LOCATION	N	Mean (mm)	Variance	LOCATION	N	Mean (mm)	Variance	LOCATION	N	Mean (mm)	Variance
N-FzL	0			FzL-LR6A	5	112.695207	0.120157	UL1I-LL1I	5	4.10686757	0.037216
N-FzR	0			FzL-LR6MB	0			UL1I-UL6MB	5	34.1661259	0.015872
N-UL1A	0			FzR-UL1A	5	79.495298	0.014158	UL1I-UR6MB	5	38.8508905	0.017598
N-UL1I	0			FzR-UL1I	5	93.4718355	0.025176	LL1A-LL1I	5	13.3424629	0.032274
N-LL1A	0			FzR-LL1A	5	102.790614	0.003743	LL1A-UL6A	5	44.4860726	0.024614
N-LL1I	0			FzR-LL1I	5	94.797234	0.062122	LL1A-LL6A	5	31.309507	0.049942
N-UL6A	0			FzR-UL6A	5	92.8631957	0.110513	LL1A-UR6A	5	45.6722266	0.071551
N-UL6MB	0			FzR-UL6MB	5	101.789043	0.033609	LL1A-LR6A	5	34.1157999	0.09792
N-LL6A	0			FzR-LL6A	5	111.703138	0.078539	LL1I-LL6MB	5	29.88731	0.069873
N-LL6MB	0			FzR-LL6MB	5	102.773779	0.116182	LL1I-LR6MB	0		
N-UR6A	0			FzR-UR6A	5	60.9837044	0.060823	UL6A-UL6MB	5	15.646643	0.054963
N-UR6MB	0			FzR-UR6MB	5	74.5510238	0.035879	UL6A-LL6A	5	28.684747	0.027538
N-LR6A	0			FzR-LR6A	5	86.8921608	0.038362	UL6A-UR6A	5	53.5944688	0.047229
N-LR6MB	0			FzR-LR6MB	0			UL6A-LR6A	5	59.8288799	0.131466
FzL-FzR	5	99.79779212	0.047518	UL1A-UL1I	5	17.6241642	0.030617	UL6MB-LL6MB	5	4.32404238	0.032692
FzL-UL1A	5	76.52128275	0.034546	UL1A-LL1A	5	33.1002625	0.016612	UL6MB-UR6MB	5	50.3940346	0.24948
FzL-UL1I	5	89.76368121	0.020758	UL1A-LL1I	5	20.5677542	0.0123	LL6A-LL6MB	5	10.4377097	0.048424
FzL-LL1A	5	100.6154734	0.022149	UL1A-UL6A	5	34.2447133	0.026774	LL6A-UR6A	5	59.1218577	0.167533
FzL-LL1I	5	91.7541917	0.075605	UL1A-UL6MB	5	36.4997802	0.012591	LL6A-LR6A	5	51.6237876	0.319874
FzL-UL6A	5	58.64391513	0.023005	UL1A-LL6A	5	45.347279	0.016813	LL6MB-LR6MB	0		
FzL-UL6MB	5	73.55247504	0.042638	UL1A-LL6MB	5	36.2870884	0.049327	UR6A-UR6MB	5	13.8788405	0.050848
FzL-LL6A	5	85.60964243	0.016141	UL1A-UR6A	5	38.6331983	0.040032	UR6A-LR6A	5	26.872463	0.017878
FzL-LL6MB	5	77.69710579	0.013053	UL1A-UR6MB	5	40.1757583	0.055404	UR6MB-LR6MB	0		
FzL-UR6A	5	95.97937141	0.064865	UL1A-LR6A	5	48.2310134	0.091622	LR6A-LR6MB	0		
FzL-UR6MB	5	103.2485766	0.207753	UL1A-LR6MB	0						

Table 13. Comparison of Sculptor™ Digital 3-D Measurements with Gold Standard (mm)
Skull A

LOCATION	Physical	Radiographic	Photographic	LOCATION	Physical	Radiographic	Photographic
Bgma-CrnaL	75.946			CrnaR-Gn	168.202	168.2685	
Bgma-CrnaR	74.192			G-ZygL	87.438	87.34709	
Bgma-G	100.596			G-ZygR	84.078	83.83432	
Bgma-ZygL	127.914			G-MasL	129.568	129.4126	
Bgma-ZygR	127.38			G-MasR	129.002	128.3341	
Bgma-MasL	143.66			G-ANS	55.296	55.48606	
Bgma-MasR	142.556			G-Gn	125.148	125.3928	
Bgma-ANS	145.124			ZygL-ZygR	120.648	120.6596	121.62597
Bgma-Gn	202.338			ZygL-MasL	59.652	59.33618	
CrnaL-CrnaR	118.18	118.8804		ZygL-MasR	125.554	125.1832	
CrnaL-G	84.482	84.48572		ZygL-ANS	80.364	80.40258	81.036252
CrnaL-ZygL	65.3	65.35745		ZygL-Gn	109.734	109.9586	110.30058
CrnaL-ZygR	134.902	135.2657		ZygR-MasL	125.88	126.1742	
CrnaL-MasL	98.786	98.81097		ZygR-MasR	62.45	61.95967	
CrnaL-MasR	146.024	146.0482		ZygR-ANS	75.938	75.63023	76.084596
CrnaL-ANS	114.692	114.8302		ZygR-Gn	107.322	107.3561	107.60326
CrnaL-Gn	165.556	165.9827		MasL-MasR	100.406	100.4502	
CrnaR-G	87.166	86.76753		MasL-ANS	115.418	115.228	
CrnaR-ZygL	138.394	138.4013		MasL-Gn	119.028	119.2434	
CrnaR-ZygR	68.392	68.19428		MasR-ANS	114.762	113.8899	
CrnaR-MasL	148.044	148.3158		MasR-Gn	119.058	118.6703	
CrnaR-MasR	99.132	98.93461		ANS-Gn	70.688	70.81487	70.757142
CrnaR-ANS	117.278	116.9307					

Table 14. Comparison of Sculptor™ Digital 3-D Measurements with Gold Standard (mm)
Skull B

LOCATION	Physical	Radiographic	Photographic	LOCATION	Physical	Radiographic	Photographic
Pclin-N	60.99	60.4541		OrbR-B	71.222	71.444	71.2078902
Pclin-OrbL	61.618	61.2005		OrbR-Gn	91.922	92.1865	92.2857605
Pclin-OrbR	62.758	62.507		OrbR-GoL	109.68	110.023	110.818226
Pclin-ANS	77.458	76.9143		OrbR-GoR	84.996	84.5938	85.4675899
Pclin-A	79.162	78.4149		OrbR-PNS	49.468	49.4933	
Pclin-Col	61.122	61.4709		ANS-A	6.842	6.61967	6.53398956
Pclin-B	103.078	102.917		ANS-CoL	95.608	95.5313	
Pclin-GoL	88.788	89.0406		ANS-PoL	109.97	110.323	
Pclin-GoR	92.046	92.2871		ANS-B	48.86	48.9549	48.7623477
N-OrbL	38.716	38.7151		ANS-Gn	71.186	71.3987	71.4154061
N-OrbR	38.88	39.0884		ANS-GoL	96.134	96.2143	96.7568361
N-A	52.584	52.7589		ANS-GoR	94.702	94.0862	94.8480306
N-CoL	96.122	96.0256		ANS-PNS	52.014	51.763	
N-PoL	107.046	107.272		A-CoL	95.246	94.9172	
N-PoR	105.136	104.38		A-PoL	109.754	109.779	
N-B	93.854	94.2212		A-B	42.354	42.4017	42.2787165
N-Gn	115.894	116.437		A-Gn	64.724	64.8474	64.939847
N-GoL	118.338	118.497		A-GoL	92.386	92.235	92.9459352
N-GoR	118.034	117.777		A-GoR	90.338	89.7173	90.6437494
N-PNS	65.328	64.9617		A-PNS	50.298	49.9127	
OrbL-OrbR	53.122	53.2053	53.0905	CoL-PoR	108.342	108.551	
OrbL-ANS	35.932	36.1345	36.0982	CoL-B	104.938	104.93	
OrbL-A	39.442	39.3072	39.3218	CoL-Gn	116.192	116.279	
OrbL-CoL	69.574	69.2526		CoL-GoL	51.758	51.7602	
OrbL-PoL	84.358	84.4974		CoL-GoR	113.586	114.205	
OrbL-PoR	111.58	111.206		CoL-PNS	62.134	62.3595	
OrbL-B	72.406	72.55	72.4422	PoL-PoR	106.356	106.863	
OrbL-Gn	92.936	93.2069	93.3157	B-Gn	22.328	22.4468	22.6698482
OrbL-GoL	86.77	86.7555	87.2772	B-GoL	79.638	79.5589	80.103911
OrbL-GoR	110.428	110.272	111.078	B-GoR	77.088	76.5007	77.1475002
OrbL-PNS	50.424	50.3151		Gn-GoL	81.462	81.4138	82.0579597
OrbR-ANS	35.308	35.1835	35.0329	Gn-GoR	78.918	78.3242	79.2107451
OrbR-A	37.934	37.8843	37.7998	Gn-PNS	78.324	78.5403	
OrbR-Col	103.102	103.361		GoL-GoR	89.68	90.1636	
OrbR-PoL	113.596	114.122					

Table 15. Comparison of Sculptor™ Digital 3-D Measurements with Gold Standard (mm)
Skull C

LOCATION	Physical	Radiographic	Photographic	LOCATION	Physical	Radiographic	Photographic
N-FzL	52.656	52.764		FzR-LR6A	86.992	86.8452	86.892161
N-FzR	52.196	52.1946		FzR-LR6MB	78.022		
N-UL1A	60.79	61.0743		UL1A-UL1I	17.482	17.4849	17.624164
N-UL1I	78.08	78.5427		UL1A-LL1A	32.9	32.8745	33.100262
N-LL1A	92.094	92.4793		UL1A-LL1I	20.462	20.3822	20.567754
N-LL1I	80.826	81.1817		UL1A-UL6A	34.068	34.0158	34.244713
N-UL6A	66.656	66.8346		UL1A-UL6MB	36.368	36.2407	36.49978
N-UL6MB	80.292	80.4638		UL1A-LL6A	45.312	45.3826	45.347279
N-LL6A	93.5	93.7907		UL1A-LL6MB	36.286	35.9674	36.287088
N-LL6MB	83.122	83.0469		UL1A-UR6A	38.95	38.6901	38.633198
N-UR6A	69.752	69.91		UL1A-UR6MB	40.126	39.9918	40.175758
N-UR6MB	81.228	81.6352		UL1A-LR6A	48.34	48.2115	48.231013
N-LR6A	94.03	94.4343		UL1A-LR6MB	38.386		
N-LR6MB	82.61			UL1I-LL1I	4.188	4.06159	4.1068676
FzL-FzR	99.262	99.459	99.7978	UL1I-UL6MB	34.172	34.0301	34.166126
FzL-UL1A	76.406	76.3093	76.5213	UL1I-UR6MB	39.146	38.7733	38.850891
FzL-UL1I	89.436	89.4976	89.7637	LL1A-LL1I	13.548	13.3592	13.342463
FzL-LL1A	100.17	100.281	100.615	LL1A-UL6A	44.054	44.1662	44.486073
FzL-LL1I	91.412	91.4095	91.7542	LL1A-LL6A	30.818	31.0812	31.309507
FzL-UL6A	58.816	58.5862	58.6439	LL1A-UR6A	45.89	45.6081	45.672227
FzL-UL6MB	73.504	73.444	73.5525	LL1A-LR6A	34.168	34.113	34.1158
FzL-LL6A	85.85	85.8534	85.6096	LL1I-LL6MB	30.284	29.6994	29.88731
FzL-LL6MB	77.434	77.4229	77.6971	LL1I-LR6MB	33.822		
FzL-UR6A	95.976	95.797	95.9794	UL6A-UL6MB	15.6	15.5038	15.646643
FzL-UR6MB	102.82	102.923	103.249	UL6A-LL6A	28.944	28.9383	28.684747
FzL-LR6A	112.38	112.497	112.695	UL6A-UR6A	53.79	53.6857	53.594469
FzL-LR6MB	102.5			UL6A-LR6A	59.698	59.8184	59.82888
FzR-UL1A	79.742	79.3757	79.4953	UL6MB-LL6MB	3.966	4.18606	4.3240424
FzR-UL1I	93.65	93.2877	93.4718	UL6MB-UR6MB	50.184	50.0616	50.394035
FzR-LL1A	102.72	102.529	102.791	LL6A-LL6MB	10.818	10.8889	10.43771
FzR-LL1I	94.93	94.6628	94.7972	LL6A-UR6A	59.192	59.2482	59.121858
FzR-UL6A	92.8	92.8697	92.8632	LL6A-LR6A	51.262	51.5326	51.623788
FzR-UL6MB	101.62	101.517	101.789	LL6MB-LR6MB	45.376		
FzR-LL6A	111.64	111.827	111.703	UR6A-UR6MB	13.958	13.8928	13.87884
FzR-LL6MB	102.84	102.693	102.774	UR6A-LR6A	27.236	26.8811	26.872463
FzR-UR6A	61.166	60.8954	60.9837	UR6MB-LR6MB	4.35		
FzR-UR6MB	74.496	74.5097	74.551	LR6A-LR6MB	11.748		

Table 16. Difference Between Sculptor™ Digital Radiographic 3-D Measurements and Gold Standard Skull A

LOCATION	Physical	Radiographic	Difference	LOCATION	Physical	Radiographic	Difference
CrnaL-CrnaR	118.18	118.88038	0.700378	G-MasR	129.002	128.3341	0.667857
CrnaL-G	84.482	84.485722	0.003722	G-ANS	55.296	55.48606	0.190055
CrnaL-ZygL	65.3	65.357452	0.057452	G-Gn	125.148	125.3928	0.244848
CrnaL-ZygR	134.902	135.2657	0.363698	ZygL-ZygR	120.648	120.6596	0.011555
CrnaL-MasL	98.786	98.810965	0.024965	ZygL-MasL	59.652	59.33618	0.315823
CrnaL-MasR	146.024	146.04823	0.024234	ZygL-MasR	125.554	125.1832	0.370832
CrnaL-ANS	114.692	114.83016	0.138156	ZygL-ANS	80.364	80.40258	0.038583
CrnaL-Gn	165.556	165.98269	0.426687	ZygL-Gn	109.734	109.9586	0.224647
CrnaR-G	87.166	86.767534	0.398466	ZygR-MasL	125.88	126.1742	0.294195
CrnaR-ZygL	138.394	138.40129	0.007288	ZygR-MasR	62.45	61.95967	0.490333
CrnaR-ZygR	68.392	68.194276	0.197724	ZygR-ANS	75.938	75.63023	0.307769
CrnaR-MasL	148.044	148.31581	0.271814	ZygR-Gn	107.322	107.3561	0.034116
CrnaR-MasR	99.132	98.934612	0.197388	MasL-MasR	100.406	100.4502	0.044242
CrnaR-ANS	117.278	116.93068	0.347324	MasL-ANS	115.418	115.228	0.190039
CrnaR-Gn	168.202	168.2685	0.066504	MasL-Gn	119.028	119.2434	0.215385
G-ZygL	87.438	87.34709	0.09091	MasR-ANS	114.762	113.8899	0.872084
G-ZygR	84.078	83.834321	0.243679	MasR-Gn	119.058	118.6703	0.387701
G-MasL	129.568	129.41261	0.155392	ANS-Gn	70.688	70.81487	0.126871

Table 17. Difference Between Sculptor™ Digital Radiographic 3-D Measurements and Gold Standard Skull B

LOCATION	Physical	Radiographic	Difference	LOCATION	Physical	Radiographic	Difference
Pclin-N	60.99	60.45414	0.53586	OrbR-B	71.22	71.444	0.222005
Pclin-OrbL	61.618	61.20045	0.41755	OrbR-Gn	91.92	92.18647	0.264465
Pclin-OrbR	62.758	62.50698	0.25102	OrbR-GoL	109.7	110.0234	0.343407
Pclin-ANS	77.458	76.91432	0.54368	OrbR-GoR	85	84.59381	0.402193
Pclin-A	79.162	78.41493	0.74707	OrbR-PNS	49.47	49.49327	0.025272
Pclin-Col	61.122	61.47088	0.34888	ANS-A	6.842	6.619665	0.222335
Pclin-B	103.08	102.9171	0.16091	ANS-CoL	95.61	95.53134	0.076664
Pclin-GoL	88.788	89.0406	0.2526	ANS-PoL	110	110.3226	0.352572
Pclin-GoR	92.046	92.28712	0.24112	ANS-B	48.86	48.95489	0.094893
N-OrbL	38.716	38.7151	0.0009	ANS-Gn	71.19	71.3987	0.212696
N-OrbR	38.88	39.08837	0.20837	ANS-GoL	96.13	96.21433	0.080328
N-A	52.584	52.75893	0.17493	ANS-GoR	94.7	94.08616	0.615839
N-CoL	96.122	96.02557	0.09643	ANS-PNS	52.01	51.76303	0.250967
N-PoL	107.05	107.2717	0.22575	A-CoL	95.25	94.9172	0.328803
N-PoR	105.14	104.3805	0.7555	A-PoL	109.8	109.7787	0.024656
N-B	93.854	94.22118	0.36718	A-B	42.35	42.40171	0.047708
N-Gn	115.89	116.4373	0.54334	A-Gn	64.72	64.84735	0.123355
N-GoL	118.34	118.4968	0.1588	A-GoL	92.39	92.23497	0.151034
N-GoR	118.03	117.7773	0.25671	A-GoR	90.34	89.7173	0.620701
N-PNS	65.328	64.96172	0.36628	A-PNS	50.3	49.91268	0.385317
OrbL-OrbR	53.122	53.20533	0.08333	CoL-PoR	108.3	108.5509	0.208887
OrbL-ANS	35.932	36.13453	0.20253	CoL-B	104.9	104.9303	0.007661
OrbL-A	39.442	39.3072	0.1348	CoL-Gn	116.2	116.279	0.086998
OrbL-CoL	69.574	69.25262	0.32138	CoL-GoL	51.76	51.76016	0.002165
OrbL-PoL	84.358	84.49736	0.13936	CoL-GoR	113.6	114.2049	0.618925
OrbL-PoR	111.58	111.2059	0.37412	CoL-PNS	62.13	62.35952	0.225523
OrbL-B	72.406	72.54996	0.14396	PoL-PoR	106.4	106.8633	0.507299
OrbL-Gn	92.936	93.20685	0.27085	B-Gn	22.33	22.44684	0.118838
OrbL-GoL	86.77	86.75546	0.01454	B-GoL	79.64	79.55891	0.079085
OrbL-GoR	110.43	110.2722	0.15575	B-GoR	77.09	76.50071	0.58729
OrbL-PNS	50.424	50.31512	0.10888	Gn-GoL	81.46	81.41377	0.048231
OrbR-ANS	35.308	35.18351	0.12449	Gn-GoR	78.92	78.3242	0.593801
OrbR-A	37.934	37.8843	0.0497	Gn-PNS	78.32	78.54025	0.216251
OrbR-Col	103.1	103.3611	0.25914	GoL-GoR	89.68	90.16355	0.483553
OrbR-PoL	113.6	114.1224	0.52636				

Table 18. Difference Between Sculptor™ Digital Radiographic 3-D Measurements and Gold Standard Skull C

LOCATION	Physical	Radiographic	Difference	LOCATION	Physical	Radiographic	Difference
N-FzL	52.656	52.76405	0.108049	FzR-UR6A	61.166	60.8954	0.270601
N-FzR	52.196	52.19463	0.001365	FzR-UR6MB	74.496	74.50969	0.013695
N-UL1A	60.79	61.07427	0.284268	FzR-LR6A	86.992	86.84523	0.146773
N-UL1I	78.08	78.54271	0.462706	UL1A-UL1I	17.482	17.48487	0.002868
N-LL1A	92.094	92.47927	0.385274	UL1A-LL1A	32.9	32.87446	0.025538
N-LL1I	80.826	81.1817	0.355701	UL1A-LL1I	20.462	20.38217	0.079826
N-UL6A	66.656	66.83458	0.178577	UL1A-UL6A	34.068	34.01582	0.052179
N-UL6MB	80.292	80.46379	0.171792	UL1A-UL6MB	36.368	36.2407	0.127301
N-LL6A	93.5	93.79069	0.290692	UL1A-LL6A	45.312	45.3826	0.070597
N-LL6MB	83.122	83.04687	0.075133	UL1A-LL6MB	36.286	35.9674	0.318597
N-UR6A	69.752	69.90997	0.157966	UL1A-UR6A	38.95	38.69013	0.259873
N-UR6MB	81.228	81.63515	0.407151	UL1A-UR6MB	40.126	39.99181	0.134189
N-LR6A	94.03	94.43434	0.404335	UL1A-LR6A	48.34	48.21149	0.128515
FzL-FzR	99.262	99.459	0.197005	UL1I-LL1I	4.188	4.061592	0.126408
FzL-UL1A	76.406	76.30933	0.096671	UL1I-UL6MB	34.172	34.03007	0.141927
FzL-UL1I	89.436	89.49758	0.061581	UL1I-UR6MB	39.146	38.77333	0.372669
FzL-LL1A	100.172	100.2814	0.109431	LL1A-LL1I	13.548	13.35917	0.188826
FzL-LL1I	91.412	91.40946	0.002542	LL1A-UL6A	44.054	44.16624	0.112244
FzL-UL6A	58.816	58.58616	0.229843	LL1A-LL6A	30.818	31.08117	0.263169
FzL-UL6MB	73.504	73.44396	0.060045	LL1A-UR6A	45.89	45.60813	0.281867
FzL-LL6A	85.85	85.85344	0.003445	LL1A-LR6A	34.168	34.11305	0.054954
FzL-LL6MB	77.434	77.42294	0.011056	LL1I-LL6MB	30.284	29.6994	0.584601
FzL-UR6A	95.976	95.79698	0.17902	UL6A-UL6MB	15.6	15.50377	0.096228
FzL-UR6MB	102.816	102.9228	0.1068	UL6A-LL6A	28.944	28.93834	0.005658
FzL-LR6A	112.376	112.4965	0.120536	UL6A-UR6A	53.79	53.6857	0.104299
FzR-UL1A	79.742	79.37569	0.366306	UL6A-LR6A	59.698	59.8184	0.120401
FzR-UL1I	93.65	93.28773	0.362268	UL6MB-LL6MB	3.966	4.186056	0.220056
FzR-LL1A	102.72	102.5292	0.190789	UL6MB-UR6MB	50.184	50.06164	0.122358
FzR-LL1I	94.93	94.6628	0.2672	LL6A-LL6MB	10.818	10.88893	0.07093
FzR-UL6A	92.8	92.86975	0.069747	LL6A-UR6A	59.192	59.24818	0.056181
FzR-UL6MB	101.618	101.5171	0.100873	LL6A-LR6A	51.262	51.53261	0.270607
FzR-LL6A	111.642	111.827	0.18502	UR6A-UR6MB	13.958	13.8928	0.065201
FzR-LL6MB	102.84	102.6929	0.147093	UR6A-LR6A	27.236	26.88107	0.354932

Table 19. Difference Between Sculptor™ Digital Photographic 3-D Measurements and Gold Standard Skull A

LOCATION	Physical	Radiographic	Difference	LOCATION	Physical	Radiographic	Difference
Bgma-CrnaL				CrnaR-Gn	168.202		
Bgma-CrnaR				G-ZygL	87.438		
Bgma-G				G-ZygR	84.078		
Bgma-ZygL				G-MasL	129.568		
Bgma-ZygR				G-MasR	129.002		
Bgma-MasL				G-ANS	55.296		
Bgma-MasR				G-Gn	125.148		
Bgma-ANS				ZygL-ZygR	120.648	121.626	0.977966
Bgma-Gn				ZygL-MasL	59.652		
CrnaL-CrnaR				ZygL-MasR	125.554		
CrnaL-G				ZygL-ANS	80.364	81.03625	0.672252
CrnaL-ZygL				ZygL-Gn	109.734	110.3006	0.566577
CrnaL-ZygR				ZygR-MasL	125.88		
CrnaL-MasL				ZygR-MasR	62.45		
CrnaL-MasR				ZygR-ANS	75.938	76.0846	0.146596
CrnaL-ANS				ZygR-Gn	107.322	107.6033	0.281256
CrnaL-Gn				MasL-MasR	100.406		
CrnaR-G				MasL-ANS	115.418		
CrnaR-ZygL				MasL-Gn	119.028		
CrnaR-ZygR				MasR-ANS	114.762		
CrnaR-MasL				MasR-Gn	119.058		
CrnaR-MasR				ANS-Gn	70.688	70.75714	0.069142
CrnaR-ANS							

Table 20. Difference Between Sculptor™ Digital Photographic 3-D Measurements and Gold Standard Skull B

LOCATION	Physical	Radiographic	Difference	LOCATION	Physical	Radiographic	Difference
Pclin-N	60.99			OrbR-B	71.22	71.20789	0.01411
Pclin-OrbL	61.618			OrbR-Gn	91.92	92.28576	0.36376
Pclin-OrbR	62.758			OrbR-GoL	109.7	110.8182	1.138226
Pclin-ANS	77.458			OrbR-GoR	85	85.46759	0.47159
Pclin-A	79.162			OrbR-PNS	49.47		
Pclin-Col	61.122			ANS-A	6.842	6.53399	0.30801
Pclin-B	103.08			ANS-CoL	95.61		
Pclin-GoL	88.788			ANS-PoL	110		
Pclin-GoR	92.046			ANS-B	48.86	48.76235	0.097652
N-OrbL	38.716			ANS-Gn	71.19	71.41541	0.229406
N-OrbR	38.88			ANS-GoL	96.13	96.75684	0.622836
N-A	52.584			ANS-GoR	94.7	94.84803	0.146031
N-CoL	96.122			ANS-PNS	52.01		
N-PoL	107.05			A-CoL	95.25		
N-PoR	105.14			A-PoL	109.8		
N-B	93.854			A-B	42.35	42.27872	0.075284
N-Gn	115.89			A-Gn	64.72	64.93985	0.215847
N-GoL	118.34			A-GoL	92.39	92.94594	0.559935
N-GoR	118.03			A-GoR	90.34	90.64375	0.305749
N-PNS	65.328			A-PNS	50.3		
OrbL-OrbR	53.122	53.09051	0.03149	CoL-PoR	108.3		
OrbL-ANS	35.932	36.09823	0.16623	CoL-B	104.9		
OrbL-A	39.442	39.32185	0.12015	CoL-Gn	116.2		
OrbL-CoL	69.574			CoL-GoL	51.76		
OrbL-PoL	84.358			CoL-GoR	113.6		
OrbL-PoR	111.58			CoL-PNS	62.13		
OrbL-B	72.406	72.4422	0.0362	PoL-PoR	106.4		
OrbL-Gn	92.936	93.31566	0.37966	B-Gn	22.33	22.66985	0.341848
OrbL-GoL	86.77	87.27722	0.50722	B-GoL	79.64	80.10391	0.465911
OrbL-GoR	110.43	111.0778	0.64985	B-GoR	77.09	77.1475	0.0595
OrbL-PNS	50.424			Gn-GoL	81.46	82.05796	0.59596
OrbR-ANS	35.308	35.03288	0.27512	Gn-GoR	78.92	79.21075	0.292745
OrbR-A	37.934	37.79983	0.13417	Gn-PNS	78.32		
OrbR-Col	103.1			GoL-GoR	89.68		
OrbR-PoL	113.6						

Table 21. Difference Between SculptorTM Digital Photographic 3-D Measurements and Gold Standard Skull C

LOCATION	Physical	Radiographic	Difference	LOCATION	Physical	Radiographic	Difference
N-FzL	52.656			FzR-LR6A	86.992	86.89216	0.099839
N-FzR	52.196			FzR-LR6MB	78.022		
N-UL1A	60.79			UL1A-UL1I	17.482	17.62416	0.142164
N-UL1I	78.08			UL1A-LL1A	32.9	33.10026	0.200262
N-LL1A	92.094			UL1A-LL1I	20.462	20.56775	0.105754
N-LL1I	80.826			UL1A-UL6A	34.068	34.24471	0.176713
N-UL6A	66.656			UL1A-UL6MB	36.368	36.49978	0.13178
N-UL6MB	80.292			UL1A-LL6A	45.312	45.34728	0.035279
N-LL6A	93.5			UL1A-LL6MB	36.286	36.28709	0.001088
N-LL6MB	83.122			UL1A-UR6A	38.95	38.6332	0.316802
N-UR6A	69.752			UL1A-UR6MB	40.126	40.17576	0.049758
N-UR6MB	81.228			UL1A-LR6A	48.34	48.23101	0.108987
N-LR6A	94.03			UL1A-LR6MB	38.386		
N-LR6MB	82.61			UL1I-LL1I	4.188	4.106868	0.081132
FzL-FzR	99.262	99.79779	0.535792	UL1I-UL6MB	34.172	34.16613	0.005874
FzL-UL1A	76.406	76.52128	0.115283	UL1I-UR6MB	39.146	38.85089	0.295109
FzL-UL1I	89.436	89.76368	0.327681	LL1A-LL1I	13.548	13.34246	0.205537
FzL-LL1A	100.172	100.6155	0.443473	LL1A-UL6A	44.054	44.48607	0.432073
FzL-LL1I	91.412	91.75419	0.342192	LL1A-LL6A	30.818	31.30951	0.491507
FzL-UL6A	58.816	58.64392	0.172085	LL1A-UR6A	45.89	45.67223	0.217773
FzL-UL6MB	73.504	73.55248	0.048475	LL1A-LR6A	34.168	34.1158	0.0522
FzL-LL6A	85.85	85.60964	0.240358	LL1I-LL6MB	30.284	29.88731	0.39669
FzL-LL6MB	77.434	77.69711	0.263106	LL1I-LR6MB	33.822		
FzL-UR6A	95.976	95.97937	0.003371	UL6A-UL6MB	15.6	15.64664	0.046643
FzL-UR6MB	102.816	103.2486	0.432577	UL6A-LL6A	28.944	28.68475	0.259253
FzL-LR6A	112.376	112.6952	0.319207	UL6A-UR6A	53.79	53.59447	0.195531
FzL-LR6MB	102.5			UL6A-LR6A	59.698	59.82888	0.13088
FzR-UL1A	79.742	79.4953	0.246702	UL6MB-LL6MB	3.966	4.324042	0.358042
FzR-UL1I	93.65	93.47184	0.178164	UL6MB-UR6MB	50.184	50.39403	0.210035
FzR-LL1A	102.72	102.7906	0.070614	LL6A-LL6MB	10.818	10.43771	0.38029
FzR-LL1I	94.93	94.79723	0.132766	LL6A-UR6A	59.192	59.12186	0.070142
FzR-UL6A	92.8	92.8632	0.063196	LL6A-LR6A	51.262	51.62379	0.361788
FzR-UL6MB	101.618	101.789	0.171043	LL6MB-LR6MB	45.376		
FzR-LL6A	111.642	111.7031	0.061138	UR6A-UR6MB	13.958	13.87884	0.07916
FzR-LL6MB	102.84	102.7738	0.066221	UR6A-LR6A	27.236	26.87246	0.363537
FzR-UR6A	61.166	60.9837	0.182296	UR6MB-LR6MB	4.35		
FzR-UR6MB	74.496	74.55102	0.055024	LR6A-LR6MB	11.748		

Table 22. Difference Between Sculptor™ Digital Radiographic and Photographic 3-D Measurements Skull A

LOCATION	Radiographic	Photographic	Difference	LOCATION	Radiographic	Photographic	Difference
Bgma-CrnaL				CrnaR-Gn	168.269		
Bgma-CrnaR				G-ZygL	87.3471		
Bgma-G				G-ZygR	83.8343		
Bgma-ZygL				G-MasL	129.413		
Bgma-ZygR				G-MasR	128.334		
Bgma-MasL				G-ANS	55.4861		
Bgma-MasR				G-Gn	125.393		
Bgma-ANS				ZygL-ZygR	120.66	121.626	0.96641
Bgma-Gn				ZygL-MasL	59.3362		
CrnaL-CrnaR	118.88			ZygL-MasR	125.183		
CrnaL-G	84.4857			ZygL-ANS	80.4026	81.03625	0.633669
CrnaL-ZygL	65.3575			ZygL-Gn	109.959	110.3006	0.341931
CrnaL-ZygR	135.266			ZygR-MasL	126.174		
CrnaL-MasL	98.811			ZygR-MasR	61.9597		
CrnaL-MasR	146.048			ZygR-ANS	75.6302	76.0846	0.454364
CrnaL-ANS	114.83			ZygR-Gn	107.356	107.6033	0.24714
CrnaL-Gn	165.983			MasL-MasR	100.45		
CrnaR-G	86.7675			MasL-ANS	115.228		
CrnaR-ZygL	138.401			MasL-Gn	119.243		
CrnaR-ZygR	68.1943			MasR-ANS	113.89		
CrnaR-MasL	148.316			MasR-Gn	118.67		
CrnaR-MasR	98.9346			ANS-Gn	70.8149	70.75714	0.057729
CrnaR-ANS	116.931						

Table 23. Difference Between Sculptor™ Digital Radiographic and Photographic 3-D Measurements
Skull B

LOCATION	Radiographic	Photographic	Difference	LOCATION	Radiograph	Photographic	Difference
Pclin-N	60.454			OrbR-B	71.44	71.20789	0.236115
Pclin-OrbL	61.2			OrbR-Gn	92.19	92.28576	0.099295
Pclin-OrbR	62.507			OrbR-GoL	110	110.8182	0.79482
Pclin-ANS	76.914			OrbR-GoR	84.59	85.46759	0.873783
Pclin-A	78.415			OrbR-PNS	49.49		
Pclin-Col	61.471			ANS-A	6.62	6.53399	0.085676
Pclin-B	102.92			ANS-CoL	95.53		
Pclin-GoL	89.041			ANS-PoL	110.3		
Pclin-GoR	92.287			ANS-B	48.95	48.76235	0.192546
N-OrbL	38.715			ANS-Gn	71.4	71.41541	0.01671
N-OrbR	39.088			ANS-GoL	96.21	96.75684	0.542508
N-A	52.759			ANS-GoR	94.09	94.84803	0.76187
N-CoL	96.026			ANS-PNS	51.76		
N-PoL	107.27			A-CoL	94.92		
N-PoR	104.38			A-PoL	109.8		
N-B	94.221			A-B	42.4	42.27872	0.122991
N-Gn	116.44			A-Gn	64.85	64.93985	0.092492
N-GoL	118.5			A-GoL	92.23	92.94594	0.710969
N-GoR	117.78			A-GoR	89.72	90.64375	0.926451
N-PNS	64.962			A-PNS	49.91		
OrbL-OrbR	53.205	53.09051	0.11481	CoL-PoR	108.6		
OrbL-ANS	36.135	36.09823	0.0363	CoL-B	104.9		
OrbL-A	39.307	39.32185	0.01465	CoL-Gn	116.3		
OrbL-CoL	69.253			CoL-GoL	51.76		
OrbL-PoL	84.497			CoL-GoR	114.2		
OrbL-PoR	111.21			CoL-PNS	62.36		
OrbL-B	72.55	72.4422	0.10776	PoL-PoR	106.9		
OrbL-Gn	93.207	93.31566	0.10881	B-Gn	22.45	22.66985	0.22301
OrbL-GoL	86.755	87.27722	0.52175	B-GoL	79.56	80.10391	0.544996
OrbL-GoR	110.27	111.0778	0.8056	B-GoR	76.5	77.1475	0.64679
OrbL-PNS	50.315			Gn-GoL	81.41	82.05796	0.644191
OrbR-ANS	35.184	35.03288	0.15063	Gn-GoR	78.32	79.21075	0.886546
OrbR-A	37.884	37.79983	0.08447	Gn-PNS	78.54		
OrbR-Col	103.36			GoL-GoR	90.16		
OrbR-PoL	114.12						

Table 24. Difference Between Sculptor™ Digital Radiographic and Photographic 3-D Measurements
Skull C

LOCATION	Radiographic	Photographic	Difference	LOCATION	Radiographi	Photographic	Difference
N-FzL	52.764			FzR-LR6A	86.845	86.89216	0.046934
N-FzR	52.1946			FzR-LR6MB			
N-UL1A	61.0743			UL1A-UL1I	17.485	17.62416	0.139297
N-UL1I	78.5427			UL1A-LL1A	32.874	33.10026	0.2258
N-LL1A	92.4793			UL1A-LL1I	20.382	20.56775	0.18558
N-LL1I	81.1817			UL1A-UL6A	34.016	34.24471	0.228892
N-UL6A	66.8346			UL1A-UL6MB	36.241	36.49978	0.259081
N-UL6MB	80.4638			UL1A-LL6A	45.383	45.34728	0.035318
N-LL6A	93.7907			UL1A-LL6MB	35.967	36.28709	0.319685
N-LL6MB	83.0469			UL1A-UR6A	38.69	38.6332	0.056929
N-UR6A	69.91			UL1A-UR6MB	39.992	40.17576	0.183947
N-UR6MB	81.6352			UL1A-LR6A	48.211	48.23101	0.019528
N-LR6A	94.4343			UL1A-LR6MB			
N-LR6MB				UL1I-LL1I	4.0616	4.106868	0.045275
FzL-FzR	99.459	99.79779	0.338787	UL1I-UL6MB	34.03	34.16613	0.136053
FzL-UL1A	76.3093	76.52128	0.211953	UL1I-UR6MB	38.773	38.85089	0.07756
FzL-UL1I	89.4976	89.76368	0.2661	LL1A-LL1I	13.359	13.34246	0.016711
FzL-LL1A	100.281	100.6155	0.334042	LL1A-UL6A	44.166	44.48607	0.319828
FzL-LL1I	91.4095	91.75419	0.344734	LL1A-LL6A	31.081	31.30951	0.228338
FzL-UL6A	58.5862	58.64392	0.057759	LL1A-UR6A	45.608	45.67223	0.064094
FzL-UL6MB	73.444	73.55248	0.10852	LL1A-LR6A	34.113	34.1158	0.002754
FzL-LL6A	85.8534	85.60964	0.243802	LL1I-LL6MB	29.699	29.88731	0.187911
FzL-LL6MB	77.4229	77.69711	0.274161	LL1I-LR6MB			
FzL-UR6A	95.797	95.97937	0.182391	UL6A-UL6MB	15.504	15.64664	0.142871
FzL-UR6MB	102.923	103.2486	0.325776	UL6A-LL6A	28.938	28.68475	0.253595
FzL-LR6A	112.497	112.6952	0.198671	UL6A-UR6A	53.686	53.59447	0.091232
FzL-LR6MB				UL6A-LR6A	59.818	59.82888	0.010479
FzR-UL1A	79.3757	79.4953	0.119604	UL6MB-LL6MB	4.1861	4.324042	0.137987
FzR-UL1I	93.2877	93.47184	0.184104	UL6MB-UR6MB	50.062	50.39403	0.332393
FzR-LL1A	102.529	102.7906	0.261403	LL6A-LL6MB	10.889	10.43771	0.45122
FzR-LL1I	94.6628	94.79723	0.134434	LL6A-UR6A	59.248	59.12186	0.126323
FzR-UL6A	92.8697	92.8632	0.006551	LL6A-LR6A	51.533	51.62379	0.09118
FzR-UL6MB	101.517	101.789	0.271916	LL6MB-LR6MB			
FzR-LL6A	111.827	111.7031	0.123882	UR6A-UR6MB	13.893	13.87884	0.013959
FzR-LL6MB	102.693	102.7738	0.080872	UR6A-LR6A	26.881	26.87246	0.008606
FzR-UR6A	60.8954	60.9837	0.088306	UR6MB-LR6MB			
FzR-UR6MB	74.5097	74.55102	0.041329	LR6A-LR6MB			